NOAA Technical Memorandum NWS WR-188

THE USE AND INTERPRETATION OF ISENTROPIC ANALYSES

Salt Lake City, Utah
October 1984

U.S. DEPARTMENT OF COMMERCE / National Oceanic and Atmospheric Administration / National Weather Service

NOAA TECHNICAL MEMORANDA
National Weather Service, Western Region Subseries

The National Weather Service (NWS) Western Region (WR) Subseries provides an informal medium for the documentation and quick dissemination of results not appropriate, or not yet ready, for formal publication. The series is used to report on work in progress, to describe technical procedures and practices, or to relate progress to a limited audience. These Technical Memoranda will report on investigations devoted primarily to regional and local problems of interest mainly to personnel, and hence will not be widely distributed.

Papers 1 to 25 are in the former series, ESSA Technical Memoranda, Western Region Technical Memoranda (WRTM); papers 24 to 59 are in the former series, ESSA Technical Memoranda, Weather Bureau Technical Memoranda (WBTM). Beginning with 60, the papers are part of the series, NOAA Technical Memorada NWS. Out-of-print memoranda are not listed.

Papers 2 to 22, except for 5 (revised edition), are available from the National Weather Service Western Region, Scientific Services Division, P. O. Box 11188, Federal Building, 125 South State Street, Salt Lake City, Utah 84147. Paper 5 (revised edition), and all others beginning with 25 are available from the National Technical Information Service, U. S. Department of Commerce, Sills Building, 5285 Port Royal Road, Springfield, Virginia 22161 Prices vary for all paper copy; $3.50 microfiche. Order by accession number shown in parentheses at end of each entry.

ESSA Technical Memoranda (WRTM)

2 Climatological Precipitation Probabilities. Compiled by Lucianne Miller, December 1965.
3 Western Region Pre- and Post-FP-3 Program, December 1, 1965, to February 20, 1966. Edward D. Diemer, March 1966.
5 Station Descriptions of Local Effects on Synoptic Weather Patterns. Philip Williams, Jr., April 1966 (revised November 1967,October 1969). (PB-17800)
8 Interpreting the RAREP. Herbert P. Benner, May 1966 (revised January 1967).
11 Some Electrical Processes in the Atmosphere. J. Latham, June 1966.
17 A Digitalized Summary of Radar Echoes within 100 Miles of Sacramento, California. J. A. Youngberg and L. B. Overaas, December 1966.
21 An Objective Aid for Forecasting the End of East Winds in the Columbia Gorge, July through October. D. John Coparanis, April 1967.
22 Derivation of Radar Horizons in Mountainous Terrain. Roger G. Pappas, April 1967.

ESSA Technical Memoranda, Weather Bureau Technical Memoranda (WBTM)

25 Verification of Operational Probability of Precipitation Forecasts, April 1966-March 1967. W. W. Dickey, October 1967. (PB-176240)
26 A Study of Winds in the Lake Mead Recreation Area. R. P. Augulis, January 1968. (PB-177830)
28 Weather Extremes. R. J. Schmidli, April 1968 (Revised December 1983)
29 Small-Scale Analysis and Prediction. Philip Williams, Jr., May 1968. (PB-178425)
30 Numerical Weather Prediction and Synoptic Meteorology. Capt. Thomas D. Murphy, U.S.A.F., May 1968. (AD-673365)
31 Precipitation Detection Probabilities by Salt Lake ARTC Radars. Robert K. Belesky, July 1968. (PB-179084)
32 Probability Forecasting--A Problem Analysis with Reference to the Portland Fire Weather District. Harold S. Ayer, July 1968. (PB-179289)
35 Joint ESSA/FAA ARTC Radar Weather Surveillance Program. Herbert P. Benner and DeVon B. Smith, December 1968 (revised June 1970). AD-681857)
36 Temperature Trends in Sacramento--Another Heat Island. Anthony D. Lentini, February 1969. (PB-183055)
37 Disposal of Logging Residues without Damage to Air Quality. Owen P. Cramer, March 1969. (PB-183057)
39 Upper-Air Lows over Northwestern United States. A. L. Jacobson, April 1969. (PB-184296)
40 The Man-Machine Mix in Applied Weather Forecasting in the 1970's. L. W. Snellman, August 1969. (PB-185068)
42 Analysis of the Southern California Santa Ana of January 15-17, 1966. Barry B. Aronovitch, August 1969. (PB-185670)
43 Forecasting Maximum Temperatures at Helena, Montana. David E. Olsen, October 1969. (PB-185762)
44 Estimated Return Periods for Short-Duration Precipitation in Arizona. Paul C. Kangieser, October 1969. (PB-187763)
46 Applications of the Net Radiometer to Short-Range Fog and Stratus Forecasting at Eugene, Oregon. L. Yee and E. Bates, December 1969. (PB-190476)
47 Statistical Analysis as a Flood Routing Tool. Robert J. C. Burnash, December 1969. (PB-188744)
48 Tsunami. Richard P. Augulis, February 1970. (PB-190157)
49 Predicting Precipitation Type. Robert J. C. Burnash and Floyd E. Hug, March 1970. (PB-190962)
50 Statistical Report on Aeroallergens (Pollens and Molds) Fort Huachuca, Arizona, 1969. Wayne S. Johnson, April 1970. (PB-191743)
51 Western Region Sea State and Surf Forecaster's Manual. Gordon C. Shields and Gerald B. Burdwell, July 1970. (PB-193102)
52 Sacramento Weather Radar Climatology. R. G. Pappas and C. M. Veliquette, July 1970. (PB-193347)
54 A Refinement of the Vorticity Field to Delineate Areas of Significant Precipitation. Barry B. Aronovitch, August 1970.
55 Application of the SSARR Model to a Basin without Discharge Record. Vail Schermerhorn and Donal W. Kuehl, August 1970. (PB-194394)
56 Areal Coverage of Precipitation in Northwestern Utah. Philip Williams, Jr., and Werner J. Heck, September 1970. (PB-194389)
57 Preliminary Report on Agricultural Field Burning vs. Atmospheric Visibility in the Willamette Valley of Oregon. Earl M. Bates and David O. Chilcote, September 1970. (PB-194710)
58 Air Pollution by Jet Aircraft at Seattle-Tacoma Airport. Wallace R. Donaldson, October 1970. (COM-71-00017)
59 Application of PE Model Forecast Parameters to Local-Area Forecasting. Leonard W. Snellman, October 1970. (COM-71-00016)

NOAA Technical Memoranda (NWS WR)

60 An Aid for Forecasting the Minimum Temperature at Medford, Oregon. Arthur W. Fritz, October 1970. (COM-71-00120)
63 700-mb Warm Air Advection as a Forecasting Tool for Montana and Northern Idaho. Norris E. Woerner, February 1971. (COM-71-00349)
64 Wind and Weather Regimes at Great Falls, Montana. Warren B. Price, March 1971.
66 A Preliminary Report on Correlation of ARTCC Radar Echoes and Precipitation. Wilbur K. Hall, June 1971. (COM-71-00829)
69 National Weather Service Support to Soaring Activities. Ellis Burton, August 1971. (COM-71-00956)
71 Western Region Synoptic Analysis-Problems and Methods. Philip Williams, Jr., February 1972. (COM-72-10433)
74 Thunderstorms and Hail Days Probabilities in Nevada. Clarence M. Sakamoto, April 1972. (COM-72-10554)
75 A Study of the Low Level Jet Stream of the San Joaquin Valley. Ronald A. Willis and Philip Williams, Jr., May 1972. (COM-72-10707)
76 Monthly Climatological Charts of the Behavior of Fog and Low Stratus at Los Angeles International Airport. Donald M. Gales, July 1972. (COM-72-11140)
77 A Study of Radar Echo Distribution in Arizona During July and August. John E. Hales, Jr., July 1972. (COM-72-11136)
78 Forecasting Precipitation at Bakersfield, California, Using Pressure Gradient Vectors. Earl T. Riddiough, July 1972. (COM-72-11146)
79 Climate of Stockton, California. Robert C. Nelson, July 1972. (COM-72-10920)
80 Estimation of Number of Days Above or Below Selected Temperatures. Clarence M. Sakamoto, October 1972. (COM-72-10021)
81 An Aid for Forecasting Summer Maximum Temperatures at Seattle, Washington. Edgar G. Johnson, November 1972. (COM-73-10150)
82 Flash Flood Forecasting and Warning Program in the Western Region. Philip Williams, Jr., Chester L. Glenn, and Roland L. Raetz, December 1972, (revised March 1978). (COM-73-10251)
83 A Comparison of Manual and Semiautomatic Methods of Digitizing Analog Wind Records. Glenn E. Rasch, March 1973. (COM-73-10669)
86 Conditional Probabilities for Sequences of Wet Days at Phoenix, Arizona. Paul C. Kangieser, June 1973. (COM-73-11264)
87 A Refinement of the Use of K-Values in Forecasting Thunderstorms in Washington and Oregon. Robert Y. G. Lee, June 1973. (COM-73-11276)
89 Objective Forecast Precipitation over the Western Region of the United States. Julia N. Paegle and Larry P. Kierulff, Sept. 1973. (COM-73-11946/3AS)
91 Arizona "Eddy" Tornadoes. Robert S. Ingram, October 1973. (COM-73-10465)
92 Smoke Management in the Willamette Valley. Earl M. Bates, May 1974. (COM-74-11277/AS)
93 An Operational Evaluation of 500-mb Type Regression Equations. Alexander E. MacDonald, June 1974. (COM-74-11407/AS)
94 Conditional Probability of Visibility Less than One-Half Mile in Radiation Fog at Fresno, California. John D. Thomas, August 1974. (COM-74-11555/AS)
96 Map Type Precipitation Probabilities for the Western Region. Glenn E. Rasch and Alexander E. MacDonald, February 1975. (COM-75-10428/AS)
97 Eastern Pacific Cut-Off Low of April 21-28, 1974. William J. Alder and George R. Miller, January 1976. (PB-250-711/AS)
98 Study on a Significant Precipitation Episode in Western United States. Ira S. Brenner, April 1976. (COM-75-10719/AS)
99 A Study of Flash Flood Susceptibility--A Basin in Southern Arizona. Gerald Williams, August 1975. (COM-75-11360/AS)
102 A Set of Rules for Forecasting Temperatures in Napa and Sonoma Counties. Wesley L. Tuft, October 1975. (PB-246-902/AS)
103 Application of the National Weather Service Flash-Flood Program in the Western Region. Gerald Williams, January 1976. (PB-253-053/AS)
104 Objective Aids for Forecasting Minimum Temperatures at Reno, Nevada, During the Summer Months. Christopher D. Hill, January 1976. (PB-252-866/AS)
105 Forecasting the Mono Wind. Charles P. Ruscha, Jr., February 1976. (PB-254-650)
106 Use of MOS Forecast Parameters in Temperature Forecasting. John C. Plankinton, Jr., March 1976. (PB-254-649)
107 Map Types as Aids in Using MOS PoPs in Western United States. Ira S. Brenner, August 1976. (PB-259-594)
108 Other Kinds of Wind Shear. Christopher D. Hill, August 1976. (PB-260-437/AS)
109 Forecasting North Winds in the Upper Sacramento Valley and Adjoining Forests. Christopher E. Fontana, September 1976. (PB-273-677/AS)
110 Cool Inflow as a Weakening Influence on Eastern Pacific Tropical Cyclones. William J. Denney, November 1976. (PB-264-655/AS)
112 The MAN/MOS Program. Alexander E. MacDonald, February 1977. (PB-265-941/AS)
113 Winter Season Minimum Temperature Formula for Bakersfield, California, Using Multiple Regression. Michael J. Oard, February 1977. (PB-273-694/AS)
114 Tropical Cyclone Kathleen. James R. Fors, February 1977. (PB-273-676/AS)
116 A Study of Wind Gusts on Lake Mead. Bradley Colman, April 1977. (PB-268-847)
117 The Relative Frequency of Cumulonimbus Clouds at the Nevada Test Site as a Function of K-Value. R. F. Quiring, April 1977. (PB-272-831)
118 Moisture Distribution Modification by Upward Vertical Motion. Ira S. Brenner, April 1977. (PB-268-740)
119 Relative Frequency of Occurrence of Warm Season Echo Activity as a Function of Stability Indices Computed from the Yucca Flat, Nevada, Rawinsonde. Darryl Randerson, June 1977. (PB-271-290/AS)

NOAA Technical Memorandum NWS WR-188

THE USE AND INTERPRETATION OF ISENTROPIC ANALYSES

Jeffrey L. Anderson

Scientific Services Division
National Weather Service Western Region
Salt Lake City, Utah
October 1984

UNITED STATES
DEPARTMENT OF COMMERCE
Malcolm Baldrige, Secretary

National Oceanic and
Atmospheric Administration
John V. Byrne, Administrator

National Weather
Service
Richard E. Hallgren, Director

This publication has been reviewed
and is approved for publication by
Scientific Services Division,
Western Region.

Glenn E. Rasch

Glenn E. Rasch, Chief
Scientific Services Division
Western Region Headquarters
Salt Lake City, Utah

TABLE OF CONTENTS

I. INTRODUCTION

The quality of short range forecasts is closely related to the forecaster's understanding of the current state of the atmoshpere in his forecast region. The vast majority of analyses of the atmosphere that are currently available to the field forecaster on AFOS are produced on constant pressure, isobaric surfaces. These charts are supplemented by analyses of surface data. Data analyses produced on isentropic charts can provide a different view of the current state of the atmosphere and can enhance the forecaster's understanding of local weather conditions. It can be argued, also, that isentropic surface analyses actually provide more useful information on a few charts than do a large array of charts produced on isobaric surfaces. While certainly not a replacement for current analysis products, isentropic surface charts can, with practice, readily supply an understanding of the state of the atmosphere that is hard to equal using isobaric charts.

Isentropic analyses of three parameters, pressure, condensation pressure, and streamlines (see Figures 2, 3, and 4), are now available on AFOS using an applications program. With practice, these charts can provide a great deal of information about the atmosphere including temperature, heights, the location of fronts and baroclinic zones, the trajectories of atmospheric parcels, the location of moist and dry tongues, the proximity of air masses to saturation, the direction of flow, and the vertical motion of atmospheric parcels. After learning to interpret the isentropic charts, the forecaster can gather information that would require numerous isobaric charts from just three isentropic charts. Isobaric charts can then be consulted for additional information in areas of active weather. Forecasters should attempt to learn the use of these isentropic charts; in many cases this should result in a better understanding of the atmosphere and better short range forecasts.

II. DEFINITIONS AND DESCRIPTION OF AN ISENTROPIC SURFACE

Isentropic charts were first used experimentally in the 1930's and found their way into operational forecasting by the early 1940's. These early isentropic charts were derived from an array of less than 50 upper air stations; data were sparse and analyses tended to be highly subjective. There was a good bit of scholarly interest in the use of isentropic charts, but operational use soon died out as constant pressure level charts became available on facsimile charts. Between the 1940's and the 1970's, the use of isentropic analysis was studied only sporadically. The advent of readily available high speed computers has again made isentropic charts a reasonable option for the operational forecaster.

An isentropic surface chart depicts meteorological parameters on a surface of constant potential temperature. Potential temperature is defined as the temperature a parcel of air would have if it were transported adiabatically to a pressure of 1000mb. This definition allows the potential temperature to be computed as $\theta = T(1000/P)^{R/C_P}$. By this definition, an isentropic surface is also a surface of constant energy and therefore a surface on which all adiabatic processes will take place.

As has been noted, all dry adiabatic processes will take place upon a single isentropic surface. This makes isentropic surfaces superior to isobaric surfaces; the exact motion of individual parcels can be traced on an isentropic surface chart but not on an isobaric chart.

Another consequence of the fact that isentropic surfaces are adiabatic surfaces is that the movement of moisture patterns can be traced easily on isentropic charts. Since an adiabatic process guarantees there will be no vertical interaction between adjacent isentropic sheets, the water vapor content of a given isentropic level must be a constant during adiabatic processes. For this reason, condensation pressure, a measure of the total water vapor content in an air parcel, should be conserved on an isentropic surface during any adiabatic process. At least theoretically, any parcel of air on an isentropic surface can be identified by its condensation pressure as it translates across the surface. Therefore, isentropic charts can provide a much better analysis of moisture patterns and their movement than can isobaric charts. Hopefully, these advantages of isentropic charts will allow field forecasters to have a better understanding of the state of the atmosphere.

III. AFOS GENERATED PRODUCTS

New software written for the AFOS computer system produces analyses of three different data fields on isentropic surfaces from significant level sounding data. The products currently available are pressure, condensation pressure, and streamlines generated from the observed winds.

To allow the forecaster to look at the most important areas of the atmosphere, the level of the isentropic surface being produced is easily variable. Being highly sensitive to the average temperature of the atmosphere below, the level of the isentrope must be varied with the seasons in order to look at areas of the atmosphere near the earth's surface. The following values are recommended as the most interesting and representative: 308K to 320K in summer, 296K to 302K in spring and autumn, and 290K to 296K in winter. While these levels will usually be the most useful, flexibility in level selection is important. Forecasters must be prepared to examine the isentropic surface that is most appropriate to their current location and weather.

The three AFOS isentropic analyses are produced by a series of interpolations on and computations with the data from significant level soundings. An examination of how the isentropic parameters are computed for a given sounding can give a better understanding of what the three analyses actually mean. This discussion will make reference to Figure 1, a SKEWT plot of Salt Lake City's sounding for 12Z on August 13, 1984. Figures 2, 3, and 4 are the corresponding isentropic plots for this sounding and will be discussed in more detail later.

Using the Salt Lake sounding, data for the 314K isentrope will be extracted by hand in a method comparable to that used by AFOS. The process begins by drawing the 314K isentrope on the sounding (Figure 1, line A). The intersection of the 314K isentrope with the sounding (point

B), gives the pressure level of the isentropic surface, approximately 800mb in this case. Notice that this is the pressure on the isentropic plot (Figure 2) for Salt Lake City.

The condensation pressure value on the isentropic surface is computed next. The point on the dewpoint sounding corresponding to the isentropic pressure (point C) is located, and the mixing ratio line from this point (line D) is drawn. Condensation pressure is defined as the pressure at which moisture in an air parcel will first condense if the parcel is cooled by lowering its pressure adiabatically. Therefore, where the mixing ratio line intersects the 314K isentrope (point E) is the level of the condensation pressure for the given parcel. For this particular sounding, the condensation pressure has a value of 650mb which agrees well with the value of condensation pressure for Salt Lake shown on the condensation pressure analysis (Figure 3).

Finally, the winds are decoded and interpolated to the same pressure level. The winds on the sounding (point F) are from the south-southwest as are the streamlines over this station in the isentropic streamline analysis (Figure 4). These computations are made for each upper air station in the analysis area in order to produce the isentropic charts.

IV. INTERPRETATION OF THE AFOS ISENTROPIC ANALYSES

Isentropic charts have generally been unavailable to field forecasters during the past three decades. While a few stations have produced isentropic charts by hand, this job was time consuming and has been performed only sporadically. AFOS has the ability to make automated isentropic charts readily available to the field forecaster.

Because they have not been commonly produced, the isentropic charts are foreign to the vast majority of forecasters. Isentropic charts are not at all like isobaric charts with which forecasters are familiar, so most forecasters will have difficulty in interpreting isentropic charts when they first confront them. With practice, however, isentropic charts can become as simple to understand as isobaric charts, and can provide more information about the state of the atmosphere. If forecasters persevere in learning to use isentropic analyses, many will find that they actually prefer these new charts to isobaric charts in certain situations.

This section examines the three new isentropic charts, both singly and in conjunction with one another. The physical interpretation of the charts will be discussed here, leaving somewhat more subjective 'forecasting rules' for section VII.

The simplest of the isentropic charts, and the one that delivers the most information by itself, is the pressure chart. Perhaps the simplest way (although not necessarily the most correct) to interpret the pressure graphic is as a 'topographic map' of the isentropic surface. In general, the lower the pressure contour on the isentropic surface, the higher the level of the surface in the atmosphere. In this way, the pressure chart can be interpretted as showing ridges and valleys that make up

the vertical displacement of the isentropic surface. As an example, Figure 2 is a pressure chart on the 314K isentropic surface at 12Z, August 13, 1984. A valley in the surface, with pressures greater than 750mb extends from the Dakotas through southern California with a closed pit found over southern California. The surface ascends on both sides of the trough, to 750mb in New Mexico, and steeply up to 530mb in northwest Washington.

Due to the definition of the isentropic surface, the pressure lines on this chart also have several other useful interpretations. The first is that the pressure lines are also isotherms on the isentropic surface. This is apparent from the definition of potential temperature, $\Theta = T(1000/P)^{R/C_P}$. Since Θ is fixed on the chart and P is fixed on the pressure lines, it is clear that T is also constant along the pressure lines. T can be computed from Θ and P by the equation $T = \Theta(1000/P)^{C_P/R}$. In Figure 2, the 750mb pressure line is also the 16°C isotherm. Areas in the Pacific Northwest and New Mexico are colder than 16°C, while the trough down the center of the analysis has warmer temperatures.

Density is also constant along the pressure lines on the isentropic surface. Since $\rho = P/RT$, and in this case, the pressure P and the temperature T are constant, the density on the pressure lines is a constant.

Thirdly, pressure lines roughly approximate lines of constant height. In Figure 2, higher height values are indicated in the Northwest than over the closed 'pit' in California. The pressure level of the isentropic surface is related directly to the mean temperature of the underlying atmospheric layer, as is the height field on a constant pressure chart.

For the same reason that they approximate height lines, the pressure lines on isentropic surfaces indicate the average temperature of the atmospheric column below the isentrope. High pressure values on the isentropic chart imply a high mean temperature in the air column; low pressure values imply a low mean temperature value. The isentropic surfaces act as excellent indicators of warm and cold tongues of air in the atmosphere. Warm tongues show up as valleys on the pressure field and cold tongues as ridges. The valley through the middle of the analysis on Figure 2 indicates a warm tongue extends through this area with colder air masses in New Mexico and the Pacific Northwest. Finally, the pressure lines are approximately parallel to the vertical shear of the geostrophic wind, the thermal wind.

The condensation pressure field indicates the moisture content of the atmosphere on the isentropic surface and helps in tracing the trajectories of individual parcels. Condensation pressure is a rarely used, but simple hydrodynamic parameter; the higher the condensation pressure, the greater the moisture content of the air. Just as regular pressure on the isentropic surface traces cold and warm tongues, the condensation pressure field traces moist and dry tongues. High values of condensation pressure imply moist tongues, and low values imply dry tongues. Figure 3 is the 314K

isentropic condensation pressure analysis for August 13, 1984, at 12Z. The condensation pressure ridge extending from Arizona and New Mexico into Utah is indicative of a moist tongue, monsoon moisture in this case. The trough over Washington and Oregon is a dry tongue which was associated with an area of subsidence behind a weak front.

As has been mentioned, during any adiabatic process moisture is confined to an isentropic sheet. Since condensation pressure is directly dependent on mixing ratio, a measure of absolute moisture, condensation pressure should be conserved with an individual parcel as the parcel translates on an isentropic surface. This rule does not hold absolutely and will be discussed later in Section VIII.

In addition to giving the absolute moisture content of a parcel, when combined with the pressure analysis, the condensation pressure can give a measure of the moisture content relative to saturation. If the pressure and condensation pressure have the same value, then the air at that point is saturated. This is apparent since air at this point does not have to be raised at all to reach saturation. Actually, due to data errors and smoothing, values of pressure and condensation pressure within 20mb of one another are indicative of saturated conditions. On the other hand, if there is a very large difference between the condensation pressure and the pressure at some point on the isentropic surface, the moisture content of the air is low. A parcel at this point must be raised a substantial distance in order to reach saturation.

There are several ways of defining quantities that indicate the proximity of air to saturation on isentropic surfaces using the pressure and condensation pressure fields. The first and most accurate is to define a quantity CP/P where CP is the condensation pressure and P the pressure on the isentropic surface. This quantity, usually referred to as the condensation ratio, is indirectly related to the relative humidity; it ranges from 0% to 100% with 100% representing a saturated parcel.

While the condensation ratio is probably the best moisture parameter that can be produced from the isentropic charts, it is extremely difficult to make analyses of the ratio. A parameter that is almost as useful, especially in the low and middle levels of the atmosphere, is what the author has defined as the condensation difference. The condensation difference is computed by subtracting the value of condensation pressure on an isentropic chart from the corresponding pressure value; this can be easily performed by doing a graphical subtraction on a condensation pressure chart overlayed on a pressure chart. The smaller the value of the condensation difference, the closer to saturation a parcel is, with a difference of less than 20mb representing saturation.

It is often useful to highlight areas of an isentropic analysis that have a pressure difference less than some threshhold value. For summer use, a difference of less than 100mb has been found to represent areas close to saturation over the West and has proved useful in tracking the flow of monsoon moisture. Figure 5, an overlay of Figures 2 and 3, shows areas of condensation difference less than 100mb as shaded. Two separate

areas of high moisture are indicated, one over Arizona, New Mexico and Colorado, and the other pushing into Nevada from central California. The first area is monsoon moisture from Mexico and the Gulf of California. The second maximum is moisture from the remains of tropical storm Iselle. Notice that both moisture maximums are hinted at in the corresponding water vapor satellite image (Figure 8).

The third field, streamlines of observed wind, produced on isentropic surfaces has not been used extensively in the past. Most earlier isentropic analysis routines have made use of the Montgomery Stream Function to produce streamlines of the gradient wind. The gradient wind as defined by the Montgomery Stream Function is entirely dependent on the value of pressure on the isentropic surface; therefore, although it depicts the pressure information in a different form, the Montgomery Stream Function provides no new information. The streamlines of observed wind, on the other hand, add an additional data source to the isentropic charts. Instead of representing the gradient winds, the streamlines of observed wind represent the actual instantaneous motion of the atmosphere as derived directly from the upper air observations. An excellent streamline contouring routine produced by NCAR allows for the production of high quality streamline charts from the sparsely distributed upper air observing sites. It appears that the observed wind streamlines are at least as useful as the gradient wind streamlines, and in certain smaller scale or highly baroclinic situations, the observed streamlines may provide a wealth of detail that the Montgomery Stream Function can not. Figure 4 is a streamline analysis on the 314K isentropic surface for August 13, 1984 at 12Z. Flow is generally from the southwest, except over New Mexico and Arizona where flow is from the southeast.

By themselves, the streamline patterns are not tremendously informative, but when combined with the pressure and condensation pressure, they provide a wealth of additional information about the state of the atmosphere. Since adiabatic processes are confined to isentropic surfaces, the streamlines indicate the actual instantaneous direction of motion of individual parcels of air. This is extremely useful for two purposes: forecasting the advection of moisture and analyzing fields of vertical motion. Initially, both of these concepts will be reviewed in a simplified fashion leaving reservations about accuracy and complicating factors for Section VIII.

A simple forecast of moisture advection can be made with relative ease using the streamlines; simply extend the current moist and dry tongue pattern along the streamlines. If isentropic analyses are being run every 12 hours, or even once a day, the use of continuity from previous charts should also be helpful in this forecast. The forecaster should readily be able to determine patterns of moisture advection from the condensation pressure charts as the moisture patterns translate along the isentropic surface. Figure 7, an overlay of Figure 3 and Figure 4, could be used to forecast advection of moisture. The streamlines from the south across Utah indicate that the moist tongue in this area will continue advecting northward into Wyoming and Idaho. Over California and Nevada, streamlines are from the southwest indicating the secondary moisture maximum in this area will be carried northeast across Idaho into Montana.

The streamline charts, when overlayed on the isentropic pressure charts, can also provide an excellent analysis of vertical motion fields. Recall that the isentropic pressure analysis gives a good approximation of the 'topography' of the isentropic surface. The streamlines, when overlayed on the pressure field, give a first approximation as to whether the air parcels are flowing up or down in the atmosphere. If the streamlines are flowing across the isobars from high pressure to lower pressure (low altitude to high altitude) then it is safe to assume there is upward vertical motion in this area. If the streamlines are flowing across the isobars from low pressure to high pressure, downward velocity is indicated, and if the streamlines are parallel to the isobars, motion is neither up nor down. Analyses of vertical velocity of this type are useful for forecasting cloudiness and stratiform precipitation in the winter and favorable areas for convection in the summer. Figure 6, an overlay of Figures 2 and 4, is a rather subtle example of analyzing vertical motion fields. Areas of weak rising motion exist from southern Nevada in a line extending to nortwest Montana and are shaded. For instance, notice that the streamline beginning off the coast of Los Angeles rises from a pressure of 833mb to less than 750mb across the shaded region.

Because the adiabatic flow on an isentropic surface must be non-divergent (any convergence or divergence is unable to result in a motion with a component perpendicular to the surface so the continuity equation would be violated), an area of convergence of streamlines on the isentropic analysis is indicative of greater wind velocity. Areas of higher velocity streamlines crossing the isobars will result in correspondingly greater upward or downward motion. The closer the streamline's crossing of the isobars is to perpendicular, and the greater the packing of the isobars, the greater the corresponding vertical motion. These facts can be used to key in on the areas of the greatest vertical velocity as depicted on the isentropic charts. Figure 6 indicates the strongest upward vertical velocity is in northern Wyoming at the top of the area of rising motion. Here, the streamlines are crossing the 750mb pressure line at nearly right angles, and the streamlines are moderately closely packed indicating an increased wind velocity.

Again, it should be stressed that most of the techniques in this section are simplified. Although these rules apply in the vast majority of cases, there are exceptions; these will be outlined later in Section VIII.

V. ISENTROPIC CHARTS AND NON-ADIABATIC PROCESSES

'Adiabatic' has been the key word in the discussion of the physical processes that are best depicted on isentropic surfaces. Processes that are not adiabatic are not depicted advantageously on the isentropic surface and have a tendency to disrupt the behavior of other processes on the isentropic charts. Three such non-adiabatic processes are convection, radiational heating or cooling, and evaporation and condensation. All three processes add energy to the atmosphere thereby forcing atmospheric parcels off of their initial isentropic surfaces. In particular, in regions of saturation parcels will follow pseudo-adiabats instead of adiabatic (isentropic) surfaces. Forecasters must use some caution when

applying isentropic analyses in regions where the air is saturated, where convection may occur, or near the ground where strong radiational heating or cooling may take place.

VI. CHOOSING THE PROPER ISENTROPIC LEVEL

One of the biggest tricks to learning to use the isentropic analysis charts is picking the proper isentropic level in the atmosphere. Levels too low will be below the surface at many locations over the analysis area; levels too high will be far above levels of interest in the atmosphere and may even become higher than the sounding data needed to produce the charts.

The programs are equipped with default level selection values for each season: 314K for summer, 299K for spring and autumn, and 293K for winter. These levels are normally close to optimal; however, several factors could influence a choice of different levels. Stations in the northern part of the United States will often wish to use colder isentropic levels so that the surfaces will not be so far aloft over their forecast region; southern stations, especially in the higher areas of the desert Southwest, will usually opt for levels warmer than the defaults to avoid having the isentropic surface intersect the earth's surface in their forecast region. Figure 2 demonstrates this concept; in southern Nevada and California, the isentropic surface is at greater than 800mb pressure, a level which would intersect certain higher areas of the surface in this region. In northwest Washington, the surface is nearly at 500mb, well above much of the more interesting weather. Abnormal temperature conditions can also cause a change in the preferred isentropic levels. Below average temperatures call for lower isentropes while above normal temperatures require higher isentropes.

Following particular meteorological phenomena may require a more precise selection of the isentropic surface. For instance, monsoon moisture flow in the Southwest has been found to occur first at levels in the vicinity of 312K to 318K. Stations affected by this flow might wish to run the isentropic analysis at one of these levels to get the earliest possible analysis of monsoon flow. It should be remembered that continuity is an important part of the use of isentropic surfaces and that levels should be varied as seldom as is possible.

VII. FORECASTING APPLICATIONS OF ISENTROPIC CHARTS

This section outlines a variety of observations about the isentopic surface analyses and their interpretation. Some of these observations include a discussion of physical processes that are responsible, others are simply the result of observations made, mostly in the 1940's, by meteorologists using isentropic charts. All of the rules outlined here should operate on scales of motion that will be depicted on the AFOS produced isentropic charts.

A. Small Scale Circulation Features

Perhaps the most useful improvement of the isentropic charts over standard isobaric surfaces is the ability to depict centers of atmospheric circulation. The isentropic charts are often able to depict circulations that are too limited, either in the horizontal or vertical dimensions to be depicted on the isobaric charts. These circulations show up as warm or cold domes on the pressure chart (depending on whether they are anticylconic or cyclonic), but are best depicted as inward or outward spiraling vortices on the isentropic streamline field. Apparently, these smaller scale features show up on isentropic surfaces because of the adiabatic nature of the surface. The actual parcels of air rotating around the circulation centers follow paths along the isentropic surface and so the streamline pattern is more likely to reveal the circulation pattern. The parcels rotating around such an area may be displaced through 100mb or more of pressure as they travel around the center; for this reason, any given isobaric chart will be unable to depict the circulation center because only part of the circulation intersects the isobar. This quality of isentropic charts is especially useful in diagnosing small scale features well south of the westerlies in summer, but it also has winter applications. Wave patterns induced by flow over varied terrain also seem to be more easily depicted by isentropic charts, again due to the adiabatic nature of the actual flow of air parcels.

The condensation pressure field also picks up details of moisture flow that are not apparent on isobaric charts. In particular, isentropic charts are excellent at depicting the flow of moisture from source regions into dynamically active regions both in winter and summer. In summer, moisture flow into convective areas can be followed; in winter, the availability of moisture to be advected into developing cyclones is shown. Isobaric charts produce inferior charts of moisture patterns because, in all but saturated parcels, the actual parcels flow along isentropic surfaces. The isobaric surface may intersect a variety of isentropic levels, and will not display the true advection patterns of moisture. The second case study in section IX demonstrates this application of the isentropic condensation pressure chart.

B. Fronts and Frontogenesis

Isentropic analyses can be very useful in determining the positions of fronts and in locating areas of potential frontogenesis or frontolysis in the atmosphere. The height of the isentrope in a region can be varied to show frontal positions at or near the surface or to analyze frontal positions at middle levels.

As anyone who has done an isentropic cross section analysis is aware, a well-developed frontal boundary tends to be nearly parallel to the isentropes and is found in an area of a strong gradient of the isentropes. By definition, fronts separate air masses of different temperature and moisture content. These two facts make isentropic surfaces valuable in frontal analysis.

The pressure field on the isentropic surface gives the most clues as to the locations of fronts. In most circumstances, a strong gradient of the pressure lines will demarcate the location of the frontal boundary; the pressure lines tend to be strongly packed behind cold fronts and ahead of strong warm fronts. The pressure lines will always be parallel to a strong front that is not decaying. If a front is known to exist, but the pressure lines on the isentropic surface are weakly spaced or cross the front, frontolysis can be assumed and the front can be forecast to weaken. Figures 9 and 10 depict hypothetical pressure fields that would be found near mature and decaying cold fronts.

The physical reasoning behind these rules is quite simple. Behind a strong cold front, one would expect to have a tongue of cold air extending along the front. This is depicted as a tongue of low pressure on the isentropic surface. Ahead of the front, with the axis of warmest air extending directly over the frontal boundary, one would expect a warm tongue which would appear as a tongue of high pressure on the isentropic chart. Naturally, between a strong band of high pressure and low pressure, there exists a strong pressure gradient parallel to the front. If there is no pressure contrast across the front on the isentropic surface, than there is no temperature contrast and the front is obviously weakening. The warm and cold tongues as depicted by the isentropic pressure field are useful in analyzing occlusions of fronts, also. Warm tongues tend to parallel the front, branching at the occlusion into two separate tongues. Figure 11 depicts a hypothetical pressure pattern over an occluding frontal system.

The isentropic pressure analysis also depicts potentially frontogenetic regions of the atmosphere. If a strong linear pressure gradient develops that is not associated with a front, it is indicative of a building air mass contrast. Often, a front will develop in this area. Because the isentropic charts depict potential frontogenetic areas and existing frontal zones in much the same way, it is usually best to employ the isentropic pressure charts to verify the position of fronts already known to exist.

The condensation pressure and streamline charts also help in identifying frontal positions. On the condensation pressure chart, a nascent front will almost always be marked by a strong moist tongue extending along the front's axis. These moist tongues are particularly useful in forecasting a developing frontal occlusion; when a front occludes, the moist tongue will often branch into two tongues, one curling cyclonically and the other anticyclonically. The occlusion is located somewhere near the branch and the heaviest precipitation is often associated with this same point. Figures 12 and 13 depict isentropic condensation pressure fields expected near a new cold front and over an occluding frontal system. Streamlines tend to converge or diverge into flow that is parallel to the front and will often depict the frontal location quite accurately. Streamlines flowing directly across a front should be regarded as a potential cause of lateral mixing and may indicate frontolysis. Figures 14 and 15 demonstrate frontogenetic and frontolytic streamline patterns.

Together the three isentropic analyses provide numerous clues as to the location of fronts. One must be careful to remember that the isentrope changes altitude over the chart, and verify that the isentrope is close enough to the surface to detect low level frontal zones. If this is done, isentropic analyses can prove a highly useful tool for locating fronts.

C. Cyclones and Cyclogenesis

Cyclones and cyclogenesis can also be depicted on isentropic charts, although this forecast skill seems to be somewhat more of an art than analyzing fronts. Again, all three charts can be used to forecast development.

The pressure field gives the clearest clues to the potential development of a low pressure system. Like fronts, cyclogenesis tends to take place at an area where there is a distinct crowding of the isobars on the isentropic pressure field. Such areas represent a developing air mass temperature contrast and therefore are a reservoir of potential energy. The most favorable area for cyclogenesis is in a pressure gradient formed between a strong cold tongue and a strong warm tongue. Cyclogenesis is expected in areas to the right of the cold tongue and anticyclogenesis to the left. Such a pattern will enable potential energy stored in the thermal contrast between the tongues to be employed in the building kinetic and thermodynamic energy of the nascent cyclone. In Figure 9, the most likely area for cyclogenesis would be near the middle of the indicated frontal boundary. Anticyclogenesis would occur behind the cold tongue, at the left side of the Figure.

The condensation pressure field indicates cyclogenesis by branching moist tongues as was mentioned in the discussion of occlusions above. The low is expected to form beneath the fork of the moist tongue which should maintain this branched form as long as the cyclone continues to develop. The streamline pattern will buckle into a trough under or just behind the area of cyclogenesis; the center of a mature cyclone should line up with the axis of the dip in the streamlines.

The isentropic charts can be a good analysis tool to search for areas of cyclogenesis and to forecast the strengthening of cyclones.

D. Non-frontal Cloudiness and Precipitation

Because they are capable of indicating proximity to saturation and areas of vertical motion, isentropic charts are excellent at predicting non-frontal cloudiness and precipitation, both in summer and in winter. Cloudiness and precipitation are generally found in moist areas, most often in areas where the moisture content is increasing. Such areas can be located by checking the twelve hour change in condensation difference on the isentropic charts. The left forward side of moist tongues has proved to be one of the most favorable areas for development of clouds and precipitation. A combination of increasing moisture, a nearly saturated air mass (low difference between pressure and condensation pressure),

and upslope motion as indicated by streamlines almost always leads to action of some sort. In summer, this action can be in the form of convection; in winter, it can generate 'isentropic' rain. 'Isentropic' rain is a term that has been used for non-frontal precipitation, generally from altostratus clouds, that falls over much of the East and Midwest at times during the winter. Isentropic charts are superior to others for forecasting precipitation events of this type.

E. Other Applications

Remembering that pressure lines are lines of constant temperature, one can use the isentropic charts to forecast the pressure level of the freezing level for aviation use. Using the relationship $\Theta = T(1000/P)^{R/C_P}$, one can compute the pressure value of the 0°C isotherm on any isentropic surface. When viewed with the condensation pressure chart to give an analysis of moisture, this can be a useful way to determine areas of possible icing. Figure 16 has a list of 0°C pressure lines for a variety of isentropic surfaces.

VIII. PROBLEMS WITH THE ISENTROPIC CHARTS

Up to this point, the discussion of the forecasting use of the isentropic analyses has always assumed the best possible scenario for the state of the atmosphere. Although the use of the isentropic charts is almost as straightforward as has been indicated, there are a few complicating factors that must be noted. Most of these complications will seldom occur and most are easy to deal with.

The vast majority of complications in the interpretation of the isentropic charts result from the translation of the entire isentropic pattern. Up to this point, it has always been assumed that the pressure field, the 'shape' of the isentropic surface, remains fixed while the pattern of condensation pressure is pushed along it by the streamline pattern. The same assumption was made in the discussion of vertical motion; the pressure pattern was assumed to be fixed while the individual air parcels flowed up or down the surface as indicated by the streamlines.

Unfortunately, it is not the case that the isentropic pressure pattern remains fixed from day to day. Instead, the pressure pattern is translated and deformed by the atmospheric flow. In the case of the pressure pattern, which is dependent on the mean temperature of the atmosphere below the isentropic surface, the translation of the pattern is dependent on the mean flow at all levels below the isentrope. Because of the translation of the pressure field, all the calculations describing the advection of the moisture pattern and the analyses of vertical motion must be modified.

At this point, the first time user of isentropic charts is on the verge of discarding these analyses as unusable because the mean flow of the air mass must first be calculated before the charts can even begin to be analyzed. Fortunately, the situation is not nearly as grim as it might appear. As long as the component of the mean wind below the isentropic surface in the direction of the streamline field on the isentropic

surface is less than the velocity of the wind on the isentropic surface, the earlier simple computations will continue to be valid. An example of this concept in the case of an area of upwards vertical velocity may help clarify this idea. If the chart shows that the streamlines are flowing from high pressure to low pressure, we have assumed upward motion. If the pressure pattern is moving in the same direction as the streamlines, but slower, the flow will still be up, but not as strongly up since the pressure pattern is moving. In almost all cases, winds increase in velocity with height, so the simple interpretation of the charts is almost always valid. In suspicious circumstances, soundings can be plotted to make sure that the mean wind velocity is not greater than the velocity of the wind on the isentropic surface.

A second complicating factor in using the isentropic charts also involves the analysis of vertical velocity. In the discussion of vertical motion, it was assumed that streamlines flowing from high pressure to low pressure were flowing upward. While this is normally the case, it need not always be so. As isobaric charts clearly demonstrate, the height of a given pressure level varies depending on the air mass. Hence, in areas of notable air mass contrast, it is possible that a decrease in pressure could actually represent a decrease in height. This situation is also relatively rare and occurs only in highly baroclinic areas, but forecasters should be aware that it can occur.

Several factors can also make the interpretation of the condensation pressure field slightly more difficult than has previously been suggested. In particular, the condensation pressure field combined with the streamlines will not give a perfect picture of the advection of the moisture pattern. Due to small scale effects, in particular the spreading out of moist tongues through lateral eddy diffusion, moist areas tend to spread out and advance more slowly than the wind velocity would indicate. Other factors, such as convection and condensation, can disrupt the continuity of the advection of the condensation pressure pattern; forecasters must be careful to keep these considerations in mind when using the isentropic charts.

A second common mistake in using the condensation pressure field is to treat the values on the chart as absolute moisture values without regard to pressure. A forecaster may see a condensation pressure of 650mb in Arizona and 350mb in Washington and assume that the Northwest is very dry. Actually, it may be the case that the pressure on the isentrope in Washington is 400mb while that in Arizona is 850mb; using the pressure difference value defined earlier, it is apparent that the air over Washington is closer to saturation than that over Arizona. It must be remembered that air's ability to hold water vapor is dependent on the air's pressure (density) so that the condensation pressure chart should always be interpreted with reference to the corresponding pressure field.

Despite this lengthy section describing problems with the interpretation of isentropic charts, it should not be assumed that they are inferior to isobaric analyses. Generally, the isentropic charts can be interpreted in the simple fashion outlined in section IV; only rarely will the more

complicated factors just discussed be important. Isobaric charts are also plagued with similar interpretation problems whose rarity has caused most forecasters to ignore them. For example, many field forecasters depend heavily on the 500mb vorticity advection to forecast vertical motion, but fail to remember that upward vertical motion is actually created by an increase in PVA with height and do not check vorticity at lower levels. The isentropic charts should be no less useful than the 500mb vorticity charts because of the problems highlighted in this section.

IX. CASE STUDIES

Two case studies, one summer situation and one winter, are appended to demonstrate some of the uses of the isentropic charts. Both cases extend over three analyses each separated by 24 hours. The summer case extends from July 23, 1984 at 12Z to July 25 at 12Z while the winter case was produced using archived data and extends from February 28, 1979 at 00Z to March 2 at 00Z.

A. Summer Case Study

This example makes use of the standard isentropic analyses that have been described in this document along with corroborating satellite pictures and isobaric charts. The isentropic fields for each analysis time are displayed in two charts. The first is the pressure field overlayed with the streamline field with areas of upward vertical motion shaded; the second is the pressure field overlayed with the condensation pressure field with areas of less than 100mb condensation difference shaded. The study examines the tracing of monsoon moisture and the forecasting of afternoon convection over the western United States.

The summer case begins with the 314K isentropic charts for July 23, 1984 at 12Z, Figures 17 and 18. Figure 19, the LFM analysis of 500mb heights and vorticity gives those unfamiliar with isentropic charts a feel for the prevailing synoptic pattern. A deep trough is nearly cut off at 130° west with a ridge over the central United States; this pattern is producing moderately strong southerly flow into California, Arizona, and northward into the great basin.

The isentropic streamline and pressure overlay, Figure 17, provides a useful analysis of the air masses and dynamics of the middle atmosphere; the pressure values range from about 650mb to less than 550mb. A weak thermal gradient extends east to west across the western United States as is indicated by lower pressures along the West Coast and steadily increasing pressures as one moves eastward. The streamlines indicate that flow is from almost due south over the entire West. Since the pressure field is so flat, this isentropic streamline field should be similar to an isobaric streamline field. Figure 20, 700mb streamlines for the same time, demonstrate that flow at this level is similar to, although a bit more westerly than, the flow on the 314K isentrope.

Areas of upward vertical velocity are shaded on Figure 17 with one area in southern Arizona and California and a second centered over Idaho. Such areas are not only indicative of upward velocity, but imply that some sort of dynamic forcing is acting. Comparison to the 500mb chart in Figure 19 shows the area of upward motion in Idaho can be associated with a vorticity maximum advecting into this area. The southern Arizona area is associated with a weaker vorticity trough that is rotating onto the coast of California. Both of these areas would be possible sites for the development of convection during the afternoon hours.

Figure 18 is an overlay of the pressure and condensation pressure analyses at 314K with areas of condensation diffence less than 100mb shaded. The shaded area indicates that much of the West is covered with moisture at this level; one tongue of apparently monsoon moisture extends northward from Arizona while a second moist tongue stretches inland from the Pacific over northern California. This pattern compares favorably with the water vapor satellite picture, Figure 21, for the same morning. The picture shows tongues of moisture over Arizona and northern California and a dry slot over southern California that matches the dry area on the isentropic chart. The streamline pattern indicates that the dry tongue should continue to push northward into Nevada gradually drying the western Great Basin. One would expect, at this time of year, convection would be likely in the middle of any of these moist areas that is associated with some dynamics.

The afternoon satellite picture, Figure 22, shows the afternoon convection pattern over the West. As can be seen, the only strong convection is in southern Arizona, possibly associated with the southern area of upward vertical motion from Figure 17. No convection has yet started in the northern vertical velocity maximum.

Figures 23 and 24 show the 314K isentropic pattern 24 hours later at 12Z on the 24th of July. The streamline-pressure chart, Figure 23, shows a warm tongue, pressure maximum, is being advected northward through Utah along the streamline flow. The whole West has warmed since the day before with pressures over the chart up about 50mb. A weak cold trough extends east-west across northern California. This area is a weak system rotating out of the trough off the West Coast as is demonstrated by the enhancement in Oregon and Washington on the water vapor image, Figure 26. Figure 23 indicates a substantially larger area of upward vertical velocity covering much of the West. The strongest values are in northern Utah and southern Arizona; note the packing of the streamlines and the perpendicular crossing of the isobars in both areas.

The pressure-condensation pressure overlay, Figure 24, shows that the dry tongue noted 24 hours earlier in southern California has continued to advect northward and now covers most of California and western Nevada. Notice that a very moist tongue with condensation pressure values close to saturation parallels the warm tongue over southern Oregon; this is additional evidence for a shortwave feature in this vicinity. The corresponding moisture picture, Figure 26, shows the dry tongue extending farther north into Idaho, but does continue to show moist maxima in Arizona and

Oregon-Washington. The initial relative humidity analysis of the LFM agress much better with the isentropic charts. Figure 25 shows the dry tongue, an area of less than 50 percent relative humidity, in California and another over Washington which is also depicted on the isentropic chart. The streamline pattern indicates that the dry tongue should continue to advect northward over Oregon and Nevada, drying out these areas.

With this pattern, one would expect convection to form in the areas of upward vertical velocity associated with high moisture; Arizona and western and northern Utah would be most favored due to the strong upward motion in these areas. More general precipitation might be expected ahead of the moist cold tongue in Oregon. The 2045Z satellite picture, Figure 27, shows that most afternoon convection has originated over orographically favored locations, however, the dynamically favored areas of Arizona and Utah appear to be the most active.

The final set of analyses is from 12Z on the 25th of July. Figure 28, pressure and streamlines on the 314K surface, shows four separate areas of upward vertical velocity over the West. The two stongest areas are in Oregon-Washington and over southern Utah-northern Arizona. The warm tongue noted 24 hours before has continued advecting north northwest with the streamline pattern and now shows as a warm maximum in Idaho. Note the area of closed pressure values in Idaho indicating a very warm air mass is found in this area. A simple look at a middle level isobaric chart for this same time would not have indicated this warm area. Figure 31, 700mb temperature analysis for this time, shows little indication of this small scale feature. It does show a stronger thermal maximum in northern Arizona, but the isentropic analysis indicates that this is not indicative of a warmer air mass.

The two areas of strongest upward velocity mentioned above are associated with quite different synoptic phenomena. The dynamics in Washington are associated with the closed low rotating off the coast as shown in Figure 32, the water vapor satellite image. The northern Arizona maximum on the other hand, is not associated with an organized feature. Figure 33, a morning IR picture, shows, however, that this area has been convectively active and is still covered with debris cloudiness.

Figure 29, the pressure-condensation pressure chart, shows the West has continued to dry from the south. The flow of monsoon moisture has also been cut, although the southeasterly streamlines in New Mexico and Arizona indicate moisture may soon be on the increase again. The 700mb dewpoint depression chart also shows this drying. See Figure 30. This chart shows a strong gradient of moisture from the very dry coast of California to still moist New Mexico. Notice that the large dewpoint depressions in California are associated with a condensation pressure minimum on the isentropic analysis as would be expected. Figure 32 also shows this strong dry area in California and Nevada and the lingering monsoon moisture farther to the east.

This study has attempted to show some simple summer applications of isentropic charts. The charts provide good analyses of air mass temperature, moisture content, and dynamics and can be used for forecasting moisture advection, dynamics, and convection.

B. Winter Case Study

The winter case study is not as involved as the summer and makes use of slightly different isentropic analyses. It was included to give a very basic introduction to some of the winter time forecasting uses of the isentropic charts. The streamline and pressure fields are the same as for the summer case. The moisture field, however, makes use of a previous version of the isentropic programs, so moisture is displayed as mixing ratio in tenths of grams/kilogram rather than as condensation pressure. Since condensation pressure is a linear function of mixing ratio, the mixing ratio field has the same shape as a corresponding condensation pressure field, but one cannot use the mixing ratio field to compute a measure of the proximity to saturation. All of the analyses are on the 293K isentropic surface and are produced from 00Z sounding data. The first analysis is for the 28th of February, 1979, and the last for the 2nd of March.

The surface and 500mb analyses for the first analysis time are found in Figures 36 and 37. The 500mb chart shows a strong mature trough is located through Colorado and into Texas with a second system digging southward off the West Coast. A cold front is analyzed at the surface curving from northern Idaho into northern California and associated with a few areas of showers. The isentropic pressure and streamline analyses, Figure 34, indicate some support for this front with a weak packing of the isobar pattern parallel to the front. A cold tongue extends southward behind the front and is shown by the lower pressures in the Pacific Northwest. A warm tongue extends northward from Arizona into Montana and is most pronounced across eastern Idaho. The most favorable area for development would be between these warm and cold tongues.

The streamlines also indicate that the front, while not tremendously energetic, should not be weakening; the flow pattern is essentially parallel to the surface frontal position. There are no pronounced areas of upward vertical motion on the whole map, so one would not expect any areas of heavy precipitation.

The pressure-mixing ratio chart, Figure 35, shows two areas of high moisture content. The first and most intense is the strong maximum in Colorado associated with the trough noted on the 500mb chart. This maximum of moisture on the isentropic chart indicates that this is a mature storm capable of producing heavy precipitation. Note, however, that the moisture maximum is entirely closed and cut off from any source region of moisture, hence one would expect this storm to be drying and weakening. The second moisture maximum is just barely depicted off the coast of northern California. It is located along the surface front as expected, and the streamlines indicate that it should continue to advect inland, providing a good moisture source for development in the dynamically favored area over Nevada. The isentropic charts indicate this is the area to watch for development during the next 24 hours.

The isentropic charts for 00Z on the 1st of March, Figures 38 and 39, indicate that the anticipated development has begun to take place in Nevada. The pressure chart shows a strong isobar gradient across Wyoming into northern Nevada that corresponds well with the frontal analysis on the surface chart, Figure 40. A double structure is now evident in the warm tongue ahead of the front with one branch in Wyoming and a second lagging behind in Nevada. The strong gradient of isobars in northern Nevada indicates a very great air mass contrast in this area which should continue to be favorable for development.

A trough has developed in the streamlines in western Nevada suggesting a cyclone may be developing ahead of this region. Vertical motion has increased over the central portion of the surface front and to the east. Virga and showers are associated with much of this area of upward motion. The mixing ratio field, Figure 39, shows a strong advection of moisture is now penetrating the West along the axis of the cold front. Note that the curves in the mixing ratio field are almost identical to the position of the surface front. The 2.1 g/kg maximum in northern California should be advected directly over the most baroclinic region on the pressure analysis and can be a moisture source for development in northern Nevada. The fact that the moist tongue is still open into the Pacific indicates that moisture advection should continue along the frontal position.

The final set of analyses is from 00Z on the 2nd of March, 1979. The pressure-streamline chart indicates that a mature and strengthening frontal system now exists in eastern Nevada. The strongest gradient of the isobars curves out of northern Wyoming and extends southward in eastern Nevada, almost directly over the position of the surface front analyzed on the 21Z chart from March 1, Figure 44. A strong consolidated warm tongue is apparent ahead of the front with an axis of high pressure along the eastern Utah border. The corresponding strong cold trough is depicted as a pressure trough from northern Idaho to southern California. These two tongues indicate that the surface front is a strong and well supported feature at this point.

The streamline pattern has now developed a deep trough with an axis in western Nevada; a feature this deep and sharp indicates excellent potential for cyclogenesis ahead of the streamline trough. The surface analysis indicates a surface low has already developed in Nevada at this time. Areas of upward vertical velocity, shaded on Figure 42, show eastern Nevada, Utah and areas further east are in areas of rising air. The two strongest areas are in northern Utah, note the strong packing of streamlines, and northern Wyoming-southern Montana where the streamlines cross the isobars at right angles. The surface map reveals precipitation is resulting in both of these areas.

The mixing ratio pattern, Figure 43, is extremely informative at this time. A very moist line is seen to parallel the surface front across Nevada. The moisture maximum is also beginning to fork into two distinct tongues which is indicative of a developing occlusion. One would anticipate further cyclogenesis under the fork with the heaviest precipitation to form under the fork (both developments did occur within the next 12 hours).

Also, the moisture tongue into the maximum has almost entirely cut off at this time. One would expect that the storm has reached its maximum moisture content and should now begin to dry out.

The winter isentropic charts are particularly adept at tracing fronts and forecasting cyclogenesis. The pressure pattern can indicate frontal positions and areas of potential development; streamlines also indicate development and provide vertical velocity patterns that are useful for forecasting precipitation. The moisture charts, mixing ratio in this particular case, may be the most useful field. The moisture indicates fronts, but is also important in forecasting the development of precipitation. The isentropic analysis of moisture advection into winter storms can be an extremely important forecast tool. Condensation pressure should prove even more useful than mixing ratio.

X. CONCLUSION

As has been demonstrated, isentropic charts can provide detailed analyses of a variety of atmospheric parameters. The pressure, condensation pressure, and streamline charts can provide analyses of air mass, temperature, moisture content, vertical motion, trajectories, and many other data fields. Together, the isentropic charts should provide more effective analyses, both in winter and summer, than can be provided by isobaric analyses. These charts have proved particularly useful in the analysis of small scale circulations, frontogenesis and fronts, cyclones and cyclogenesis, and non-frontal cloudiness and precipitation. Three isentropic charts can provide the information supplied by numerous isobaric charts. Although the isentropic charts will seem foreign to many users of isobaric charts, practice with isentropic charts will soon make them as easy to interpret. Hopefully, forecasters will use isentropic charts to obtain a better knowledge of the state of the atmosphere and this will in turn result in better forecasts.

XI. REFERENCES

1 Anderson, Jeffrey L., "Mesoscale Objective Analysis", NOAA Western Region Computer Programs and Problems NWS WRCP - No. 33, 1983.

2 Anderson, Jeffrey L., "Isentropic Objective Analysis", NOAA Western Region Computer Programs and Problems NWS WRCP - No. 47, 1984.

3 Berry, F.A., Handbook of Meteorology, McGraw-Hill Inc., New York, 1945.

4 Byers, Horace R., General Meteorology, McGraw-Hill Inc., New York, 1944.

5 Byers, Horace R., "On the Thermodynamic Interpretation of Isentropic Charts", Monthly Weather Review, 66:63-68, March, 1938.

6 Holton, James R., An Introduction to Dynamic Meteorology, Academic Press, New York, 1979.

7 Montgomery, R.B., "A Suggested Method for Representing Gradient Flow in Isentropic Surfaces", Bulletin American Meteorological Society, 18:210-212, June, 1938.

8 Namias, Jerome, and others, Air Mass and Isentropic Analysis, American Meteorological Society, Milton, Mass., 1940.

9 Newton, C.W., "Mechanisms of Circulation Change During a Lee Cyclogenesis", Journal of Meteorology, 13:528-539, 1956.

10 Shapiro, M.A., "The Use of Isentropic Coordinates in the Formulation of Objective Analysis and Numerical Prediction Models", NCAR, Boulder, 1984.

11 Shaw, Napier, Manual of Meteorology, Vol, III, Cambridge University Press, Cambridge, 1942.

12 Uccellini, L.W., P.J. Kocin, R.A. Petersen, C. H. Wash, and K. F. Brill, 1984: "The Presidents' Day Cyclone of 18-19 February 1979: Synoptic Overview and Analysis of Subtropical Jet Streak Influencing the Pre-Cyclogenetic Period. Monthly Weather Review., 112 (January issue).

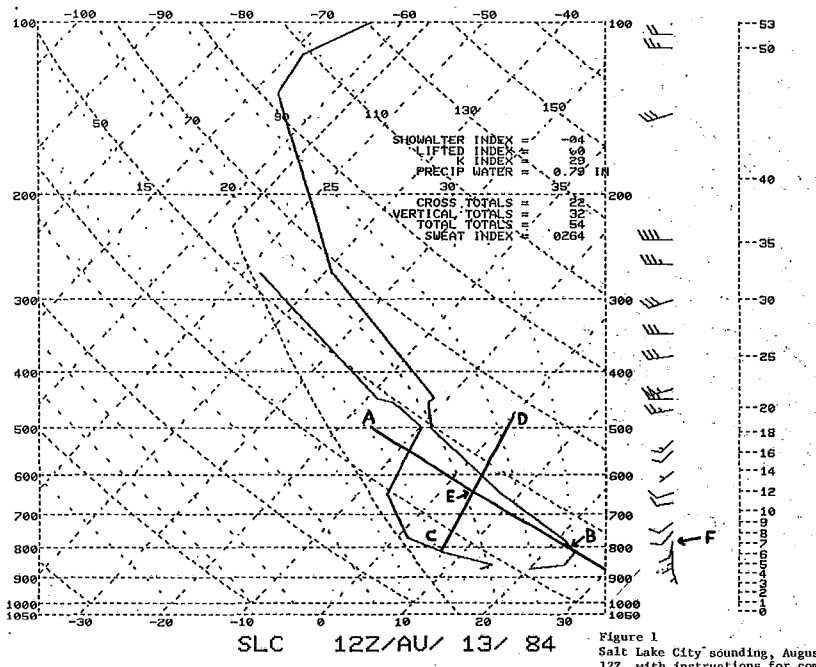

Figure 1
Salt Lake City sounding, August 13, 1984, 12Z, with instructions for computing isentropic surface values.

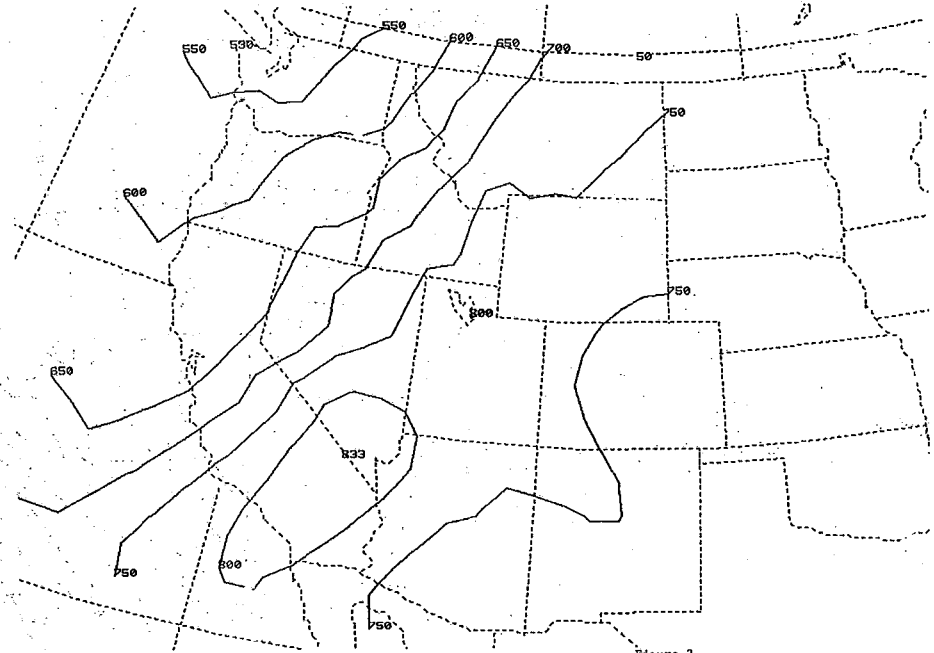

Figure 2
314K Isentropic pressure field for 12Z, August 13, 1984.

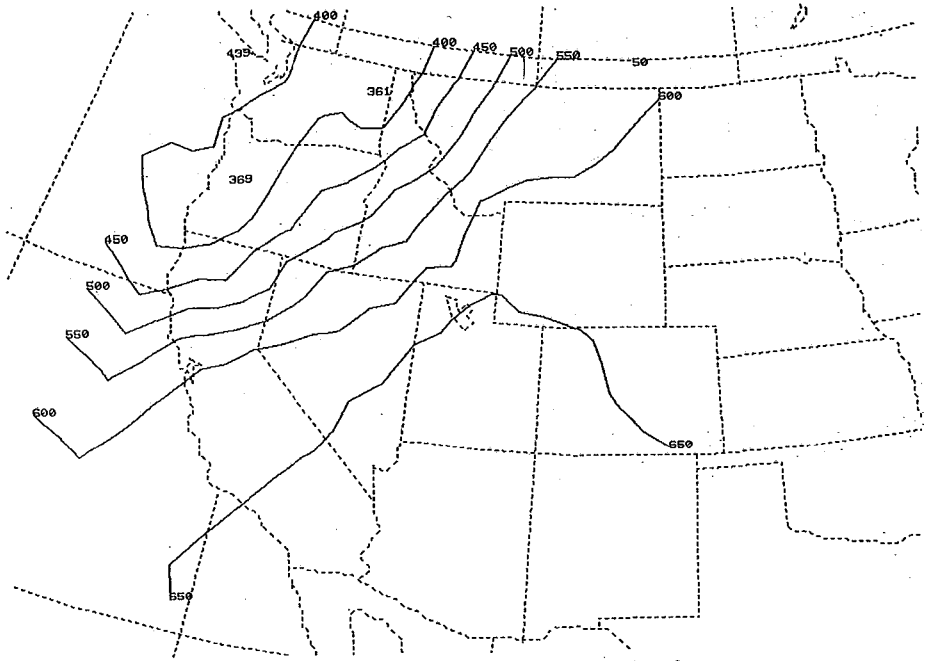

Figure 3
314K Condensation pressure analysis for 12Z, August 13, 1984.

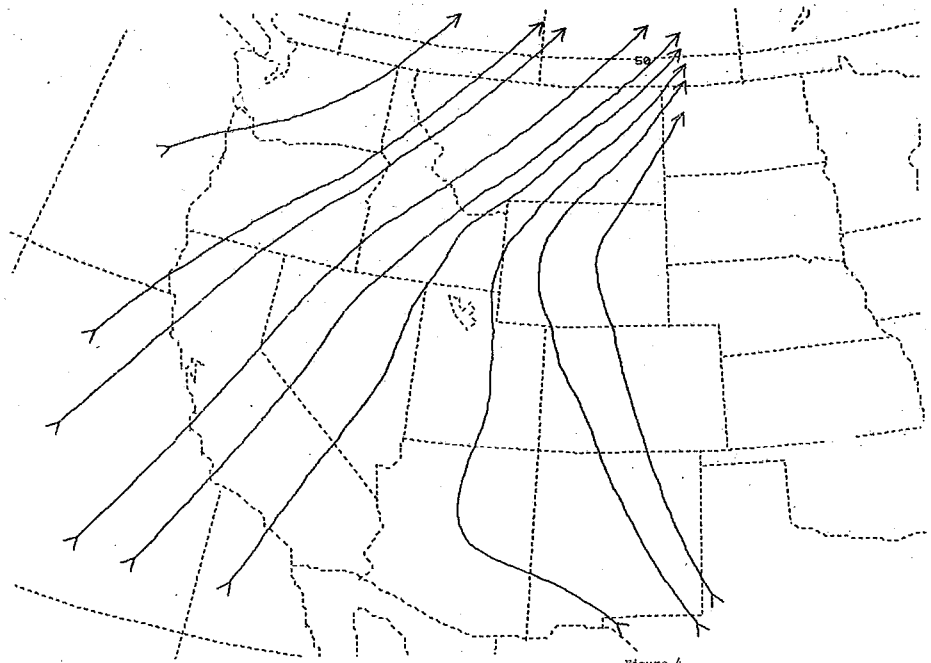

Figure 4
314K Streamlines for 12Z, August 13, 1984.

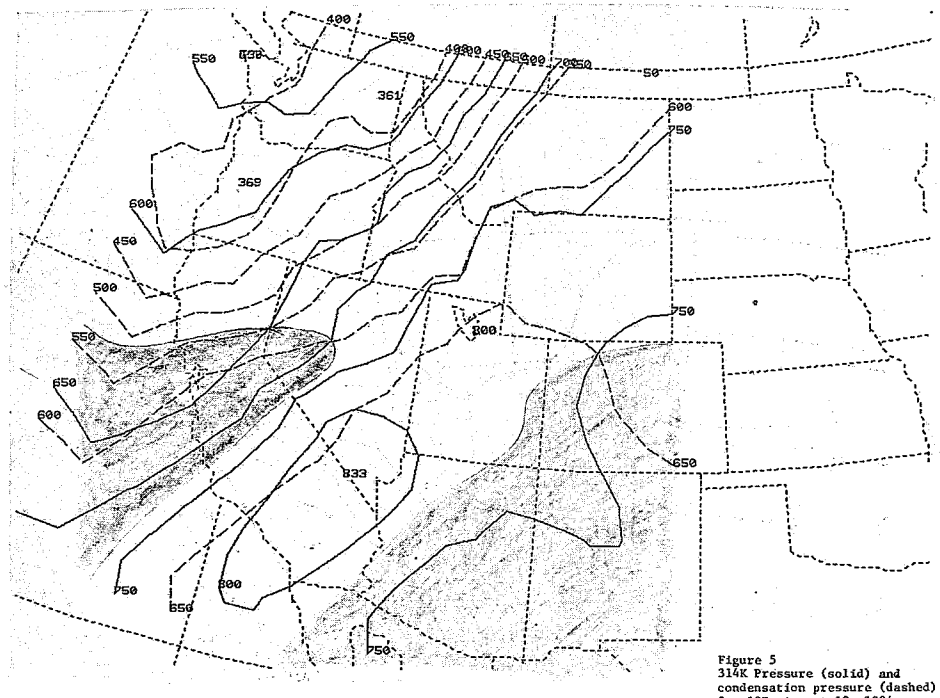

Figure 5
314K Pressure (solid) and condensation pressure (dashed) for 12Z, August 13, 1984.

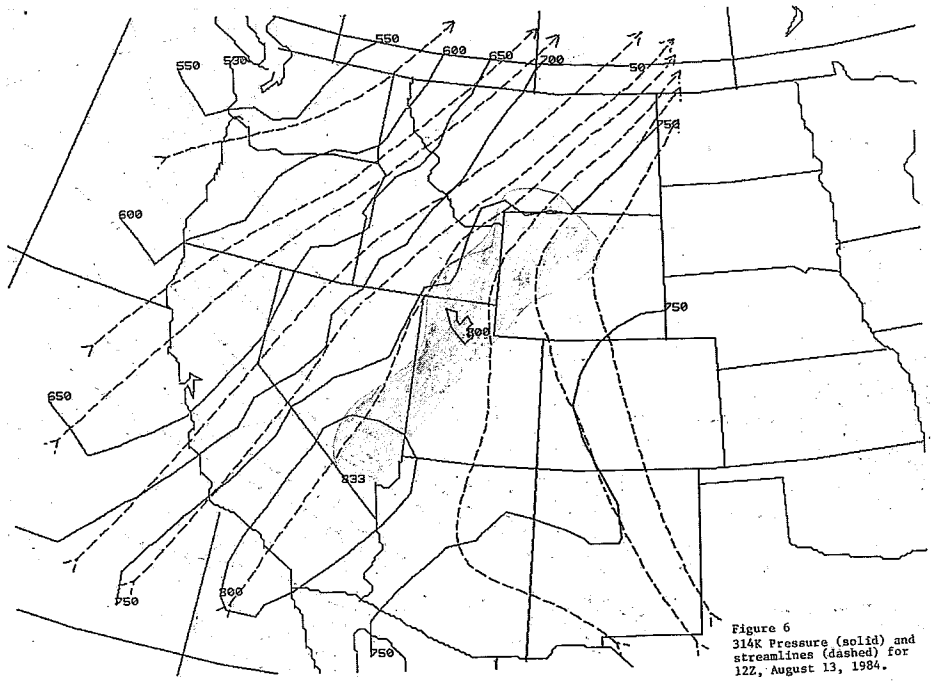

Figure 6
314K Pressure (solid) and streamlines (dashed) for 12Z, August 13, 1984.

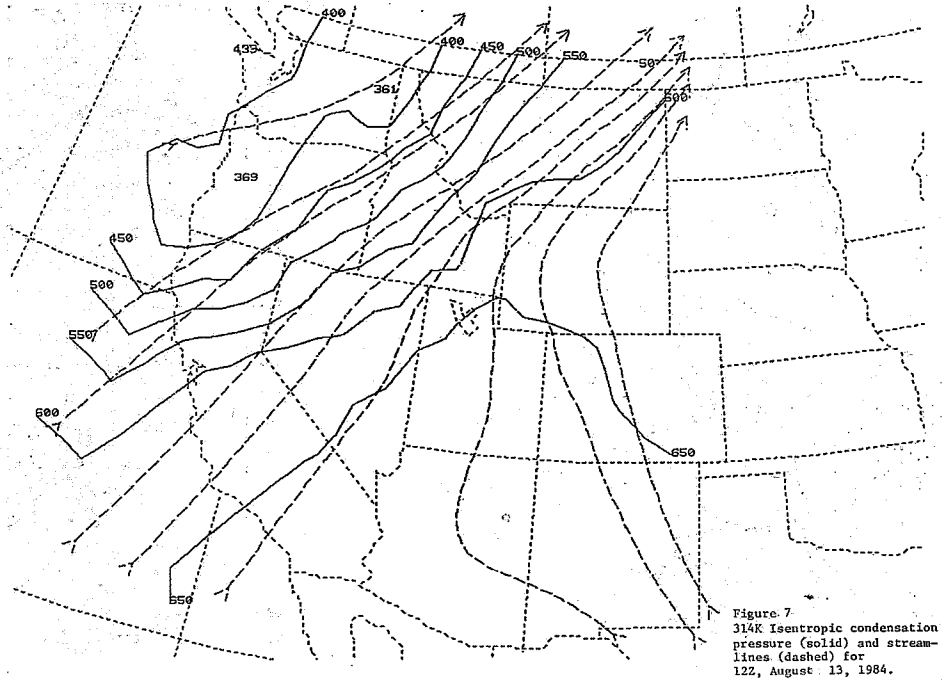

Figure 7
314K Isentropic condensation pressure (solid) and streamlines (dashed) for 12Z, August 13, 1984.

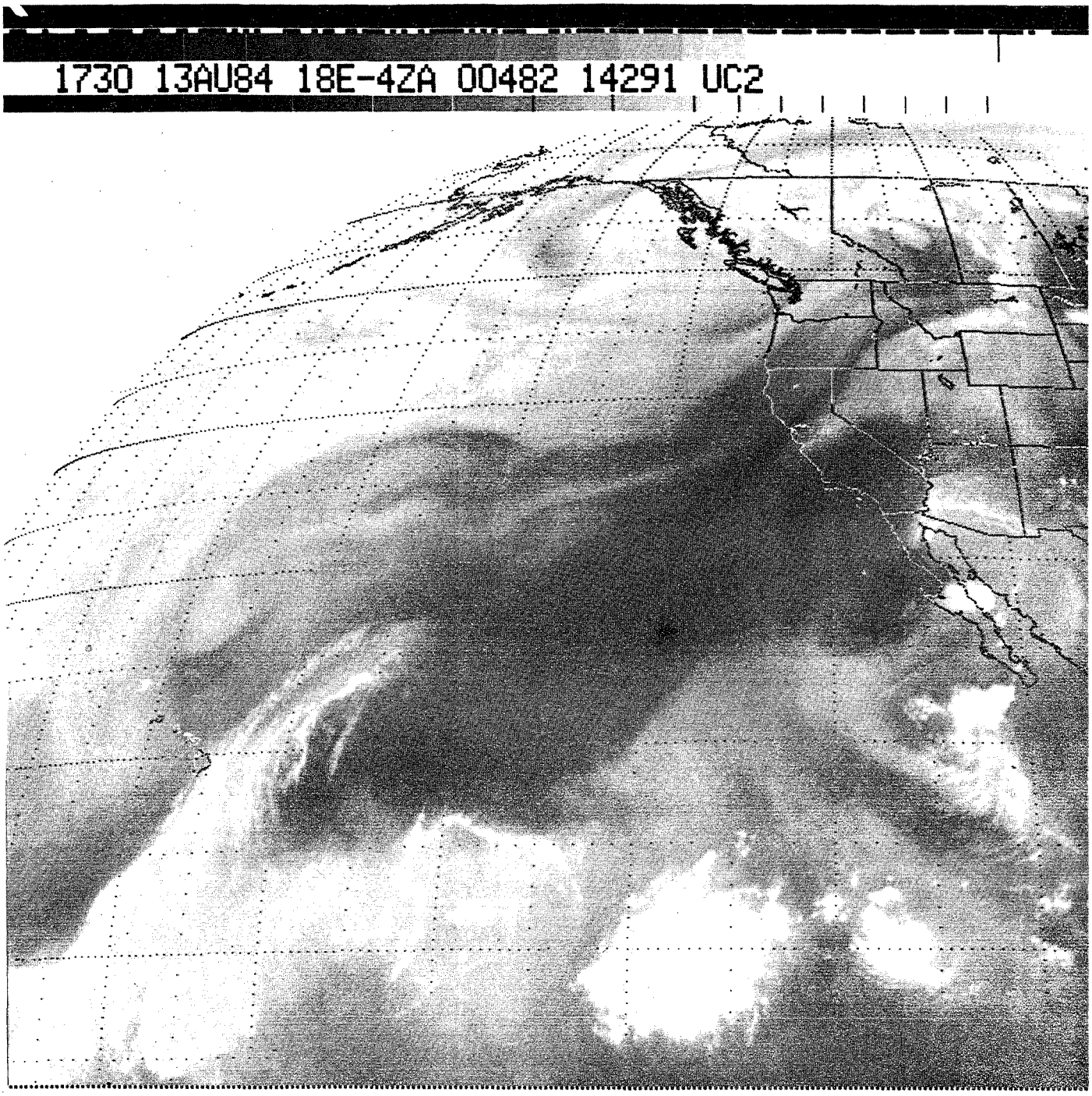

Figure 8
1730Z Moisture picture for
August 13, 1984.

Figure 9
Isentropic pressure pattern in the vicinity of a strong, mature cold front.

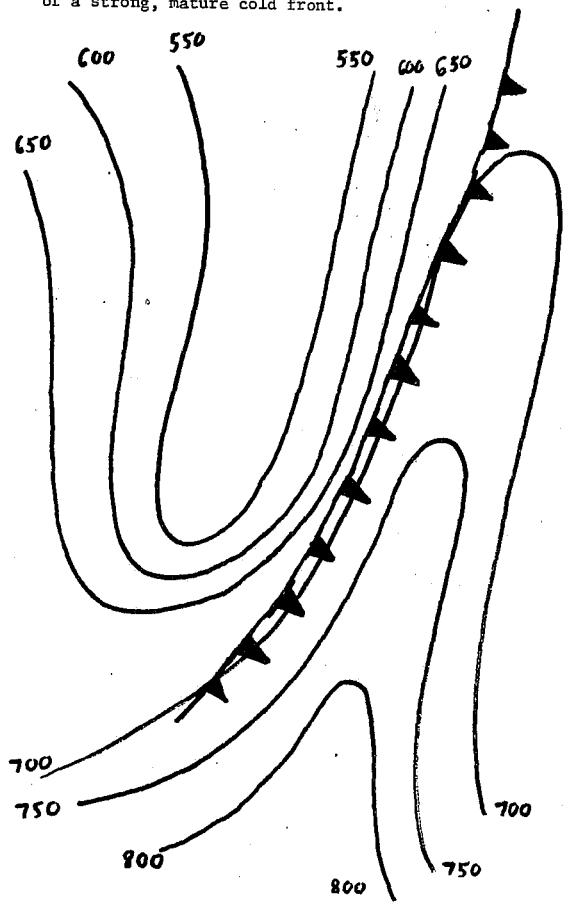

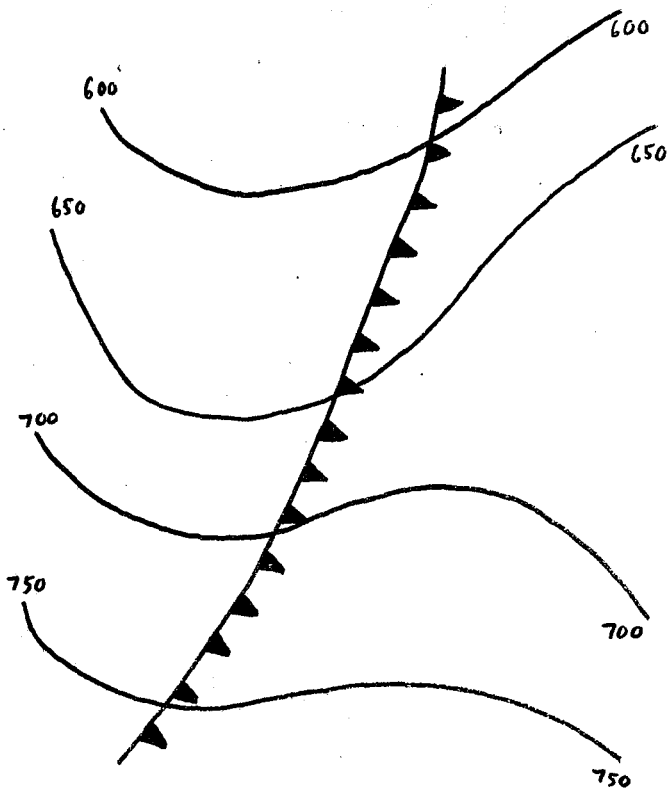

Figure 10
Isentropic pressure pattern in vicinity of a frontolysizing cold front.

Figure 11
Isentropic pressure pattern in vicinity of an occluding frontal system.

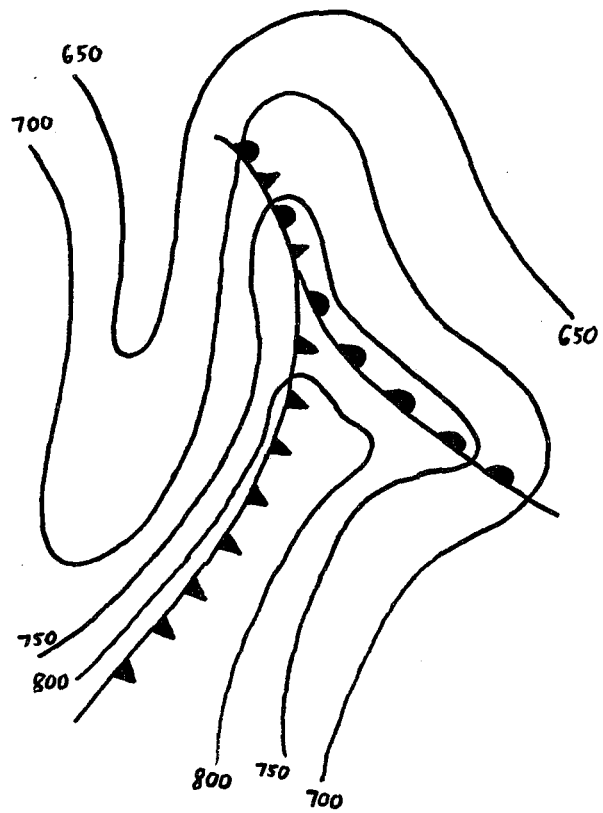

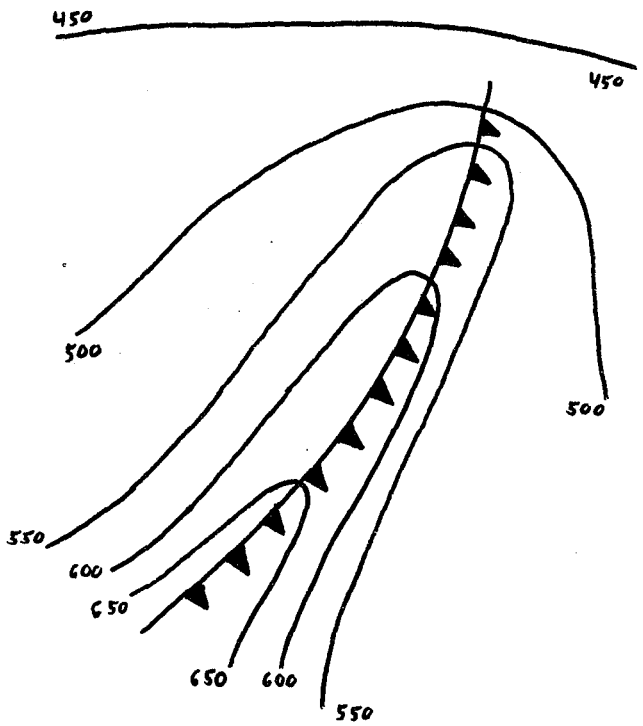

Figure 12
Isentropic condensation pressure pattern over a mature, strong cold front.

Figure 13
Isentropic condensation pressure pattern over an occluding frontal system.

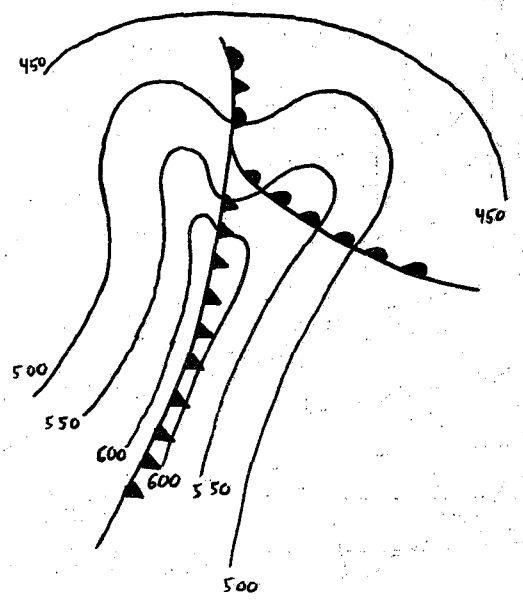

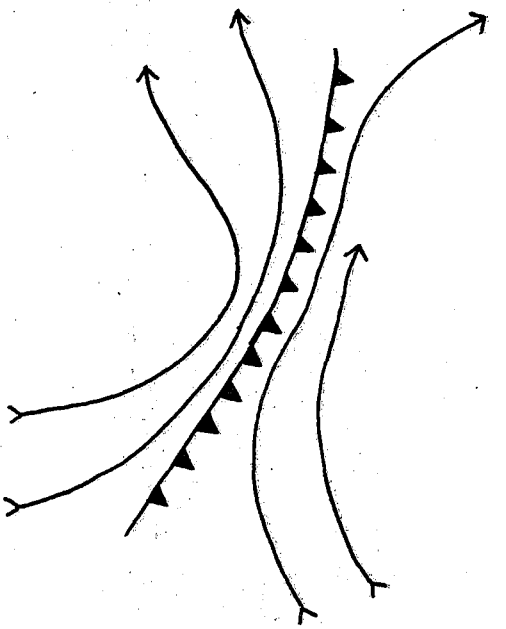

Figure 14
Isentropic streamlines in vicinity of a strengthening cold front.

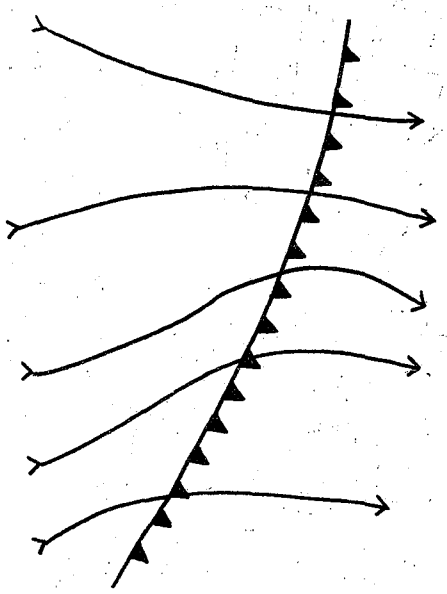

Figure 15
Isentropic streamlines over a weakening cold front.

POTENTIAL TEMP	PRESSURE OF FREEZING LEVEL	POTENTIAL TEMP	PRESSURE OF FREEZING LEVEL
290	809	306	671
291	800	307	663
292	790	308	656
293	781	309	648
294	772	310	641
295	762	311	634
296	753	312	627
297	745	313	620
298	736	314	613
299	727	315	606
300	719	316	599
301	711	317	593
302	702	318	586
303	694	319	580
304	686	320	576
305	678		

Figure 16
Pressure values of $0^{\circ}C$ isotherm for various isentropic surfaces.

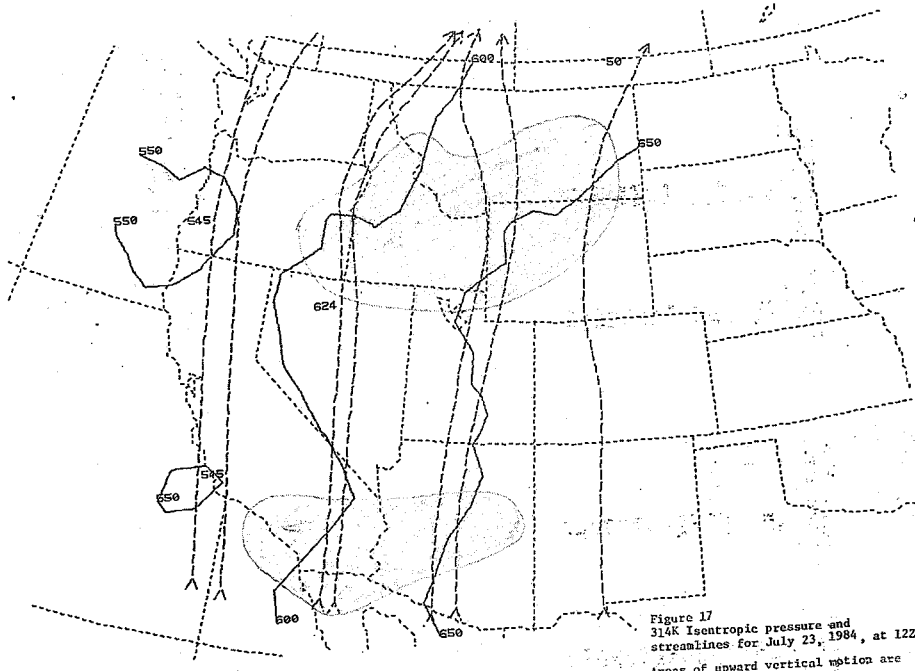

Figure 17
314K Isentropic pressure and streamlines for July 23, 1984, at 12Z.

Areas of upward vertical motion are shaded.

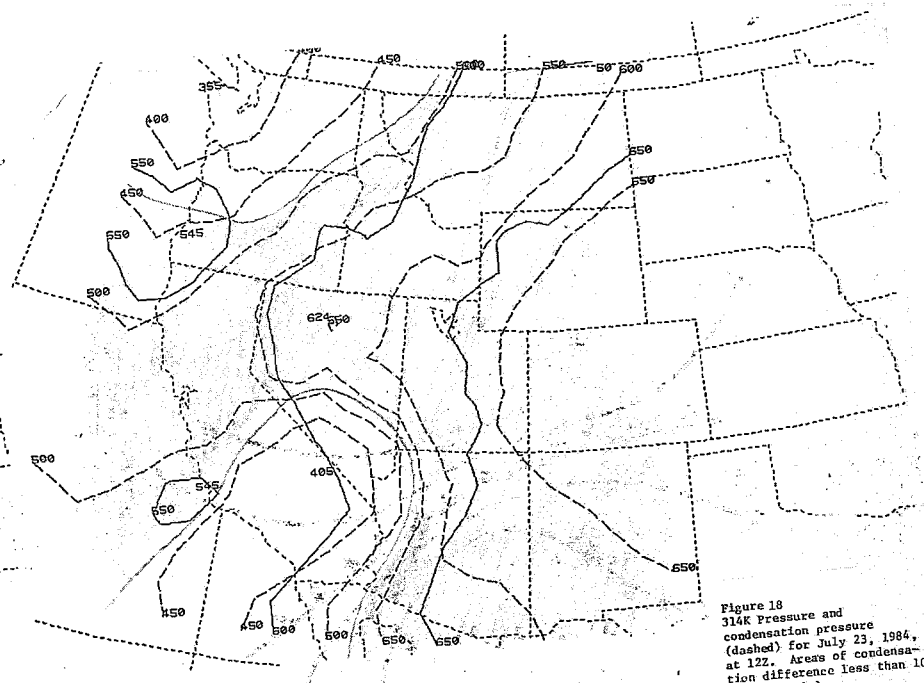

Figure 18
314K Pressure and condensation pressure (dashed) for July 23, 1984, at 12Z. Areas of condensation difference less than 100 mb are shaded.

Figure 19
500 mb LFM analysis of heights and vorticity for 12Z, July 23, 1984.

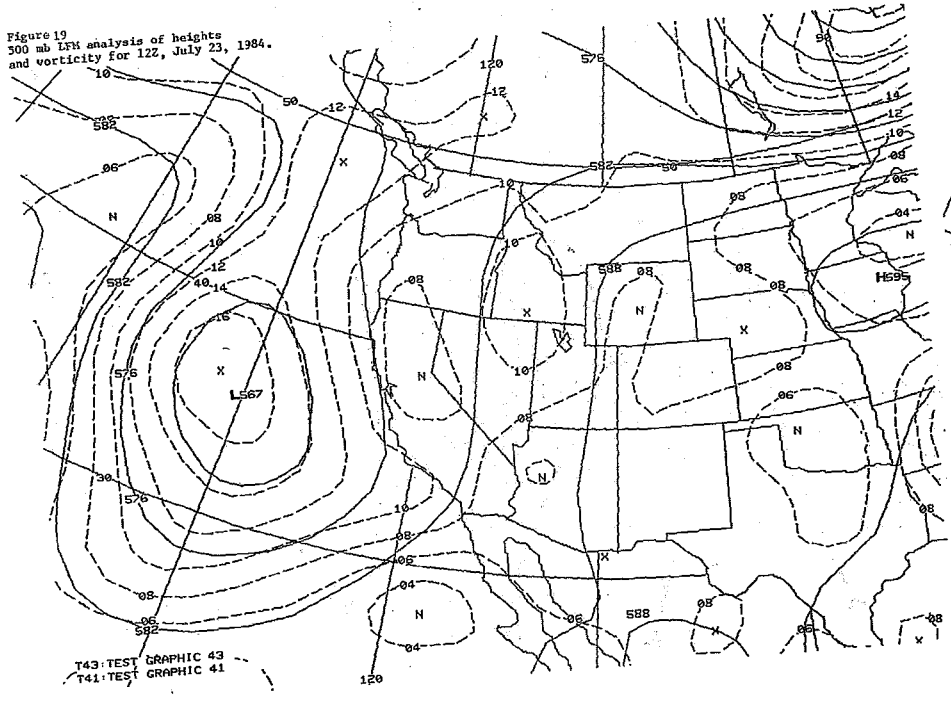

T43:TEST GRAPHIC 43
T41:TEST GRAPHIC 41

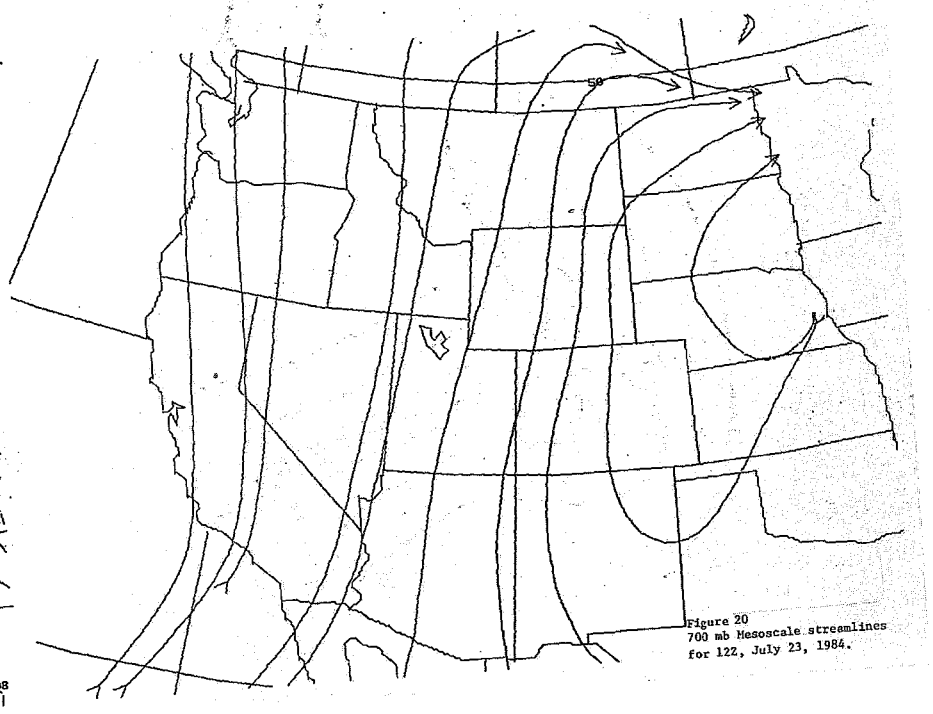

Figure 20
700 mb Mesoscale streamlines for 12Z, July 23, 1984.

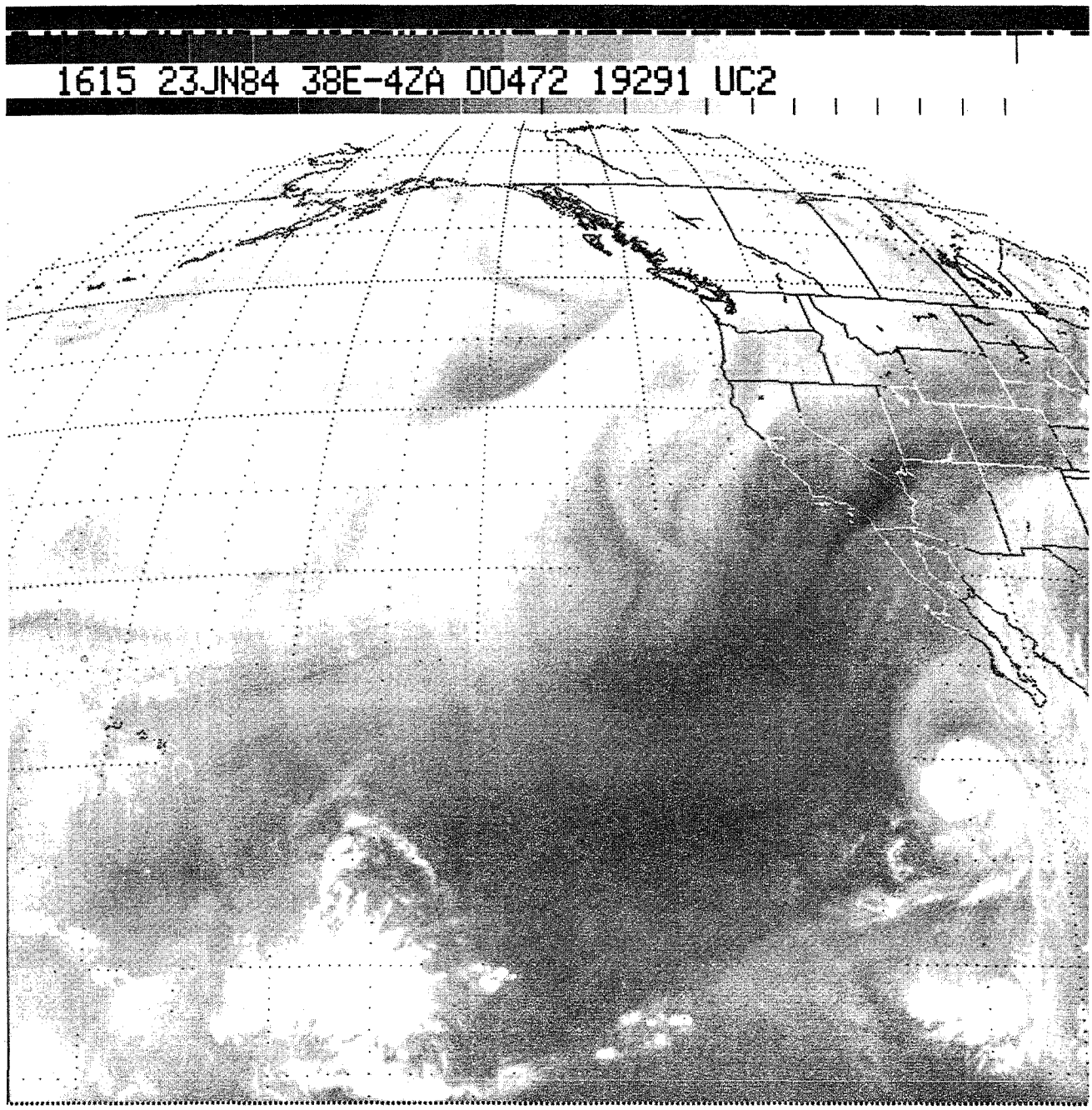

Figure 21
Water vapor picture for
1615Z, June 23, 1984.

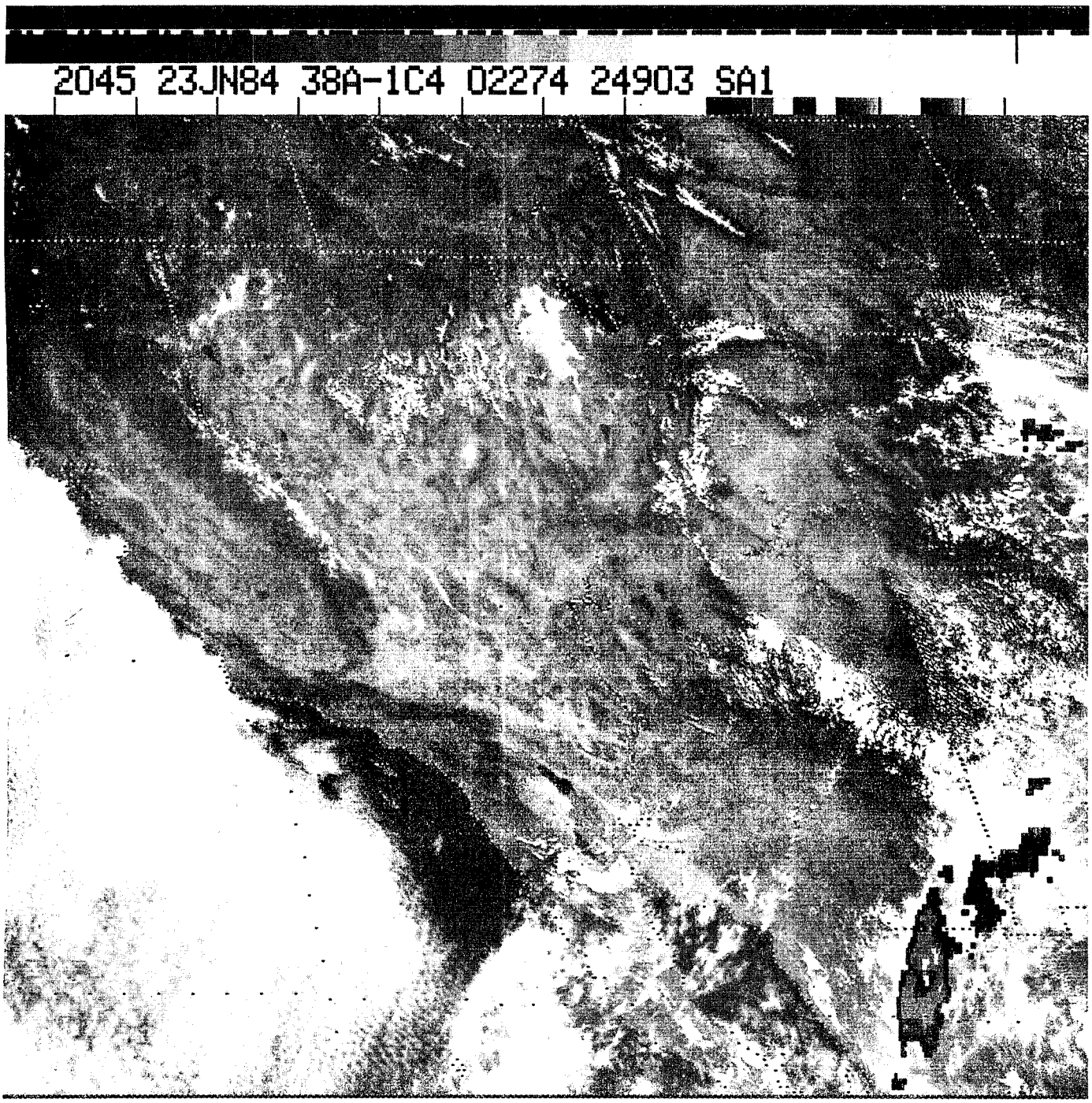

Figure 22
2045Z enhanced visible satellite image for June 23, 1984.

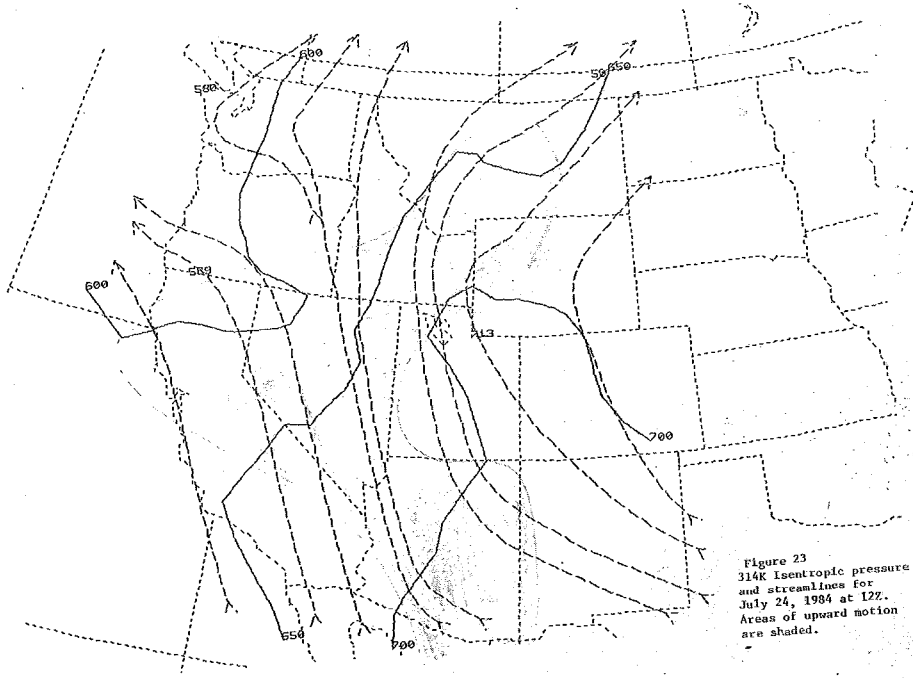

Figure 23
314K Isentropic pressure and streamlines for July 24, 1984 at 12Z. Areas of upward motion are shaded.

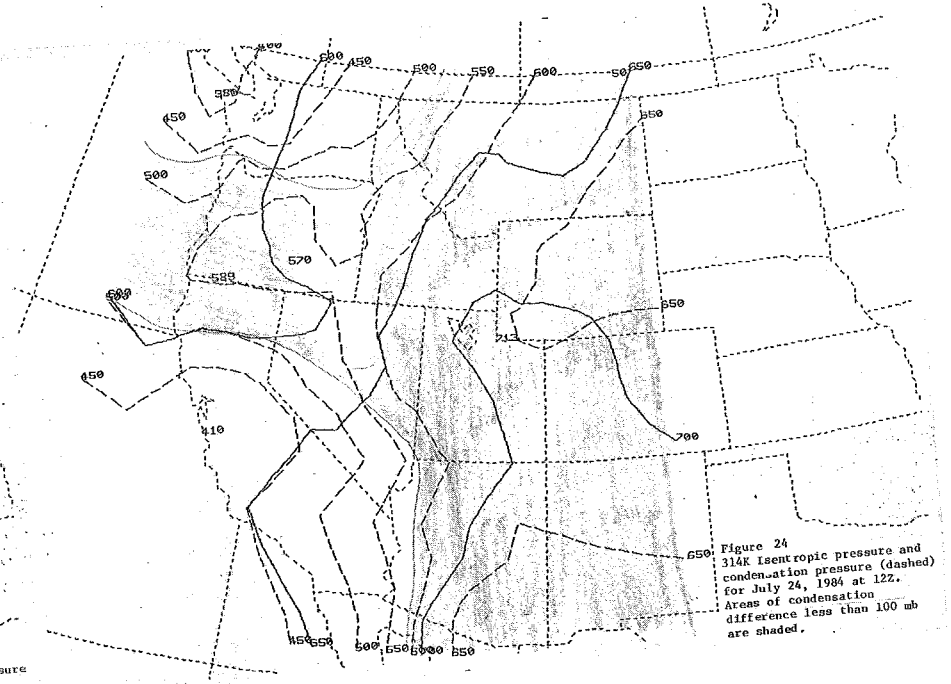

Figure 24
314K Isentropic pressure and condensation pressure (dashed) for July 24, 1984 at 12Z. Areas of condensation difference less than 100 mb are shaded.

Figure 25
LFM Relative humidity analysis for July 24, 1984 at 12Z.

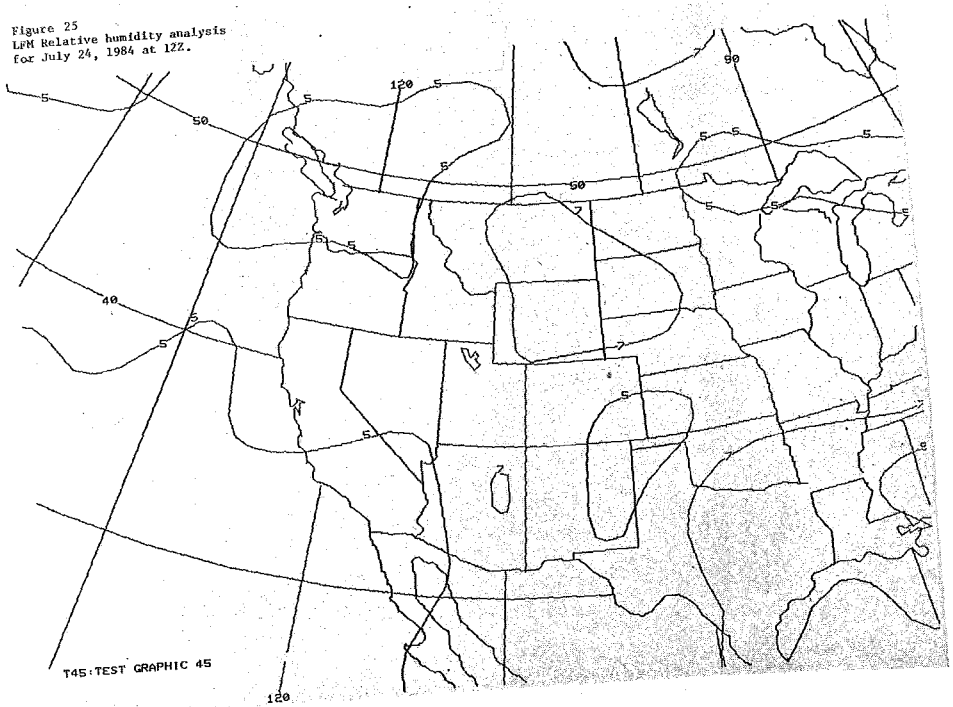

T45:TEST GRAPHIC 45

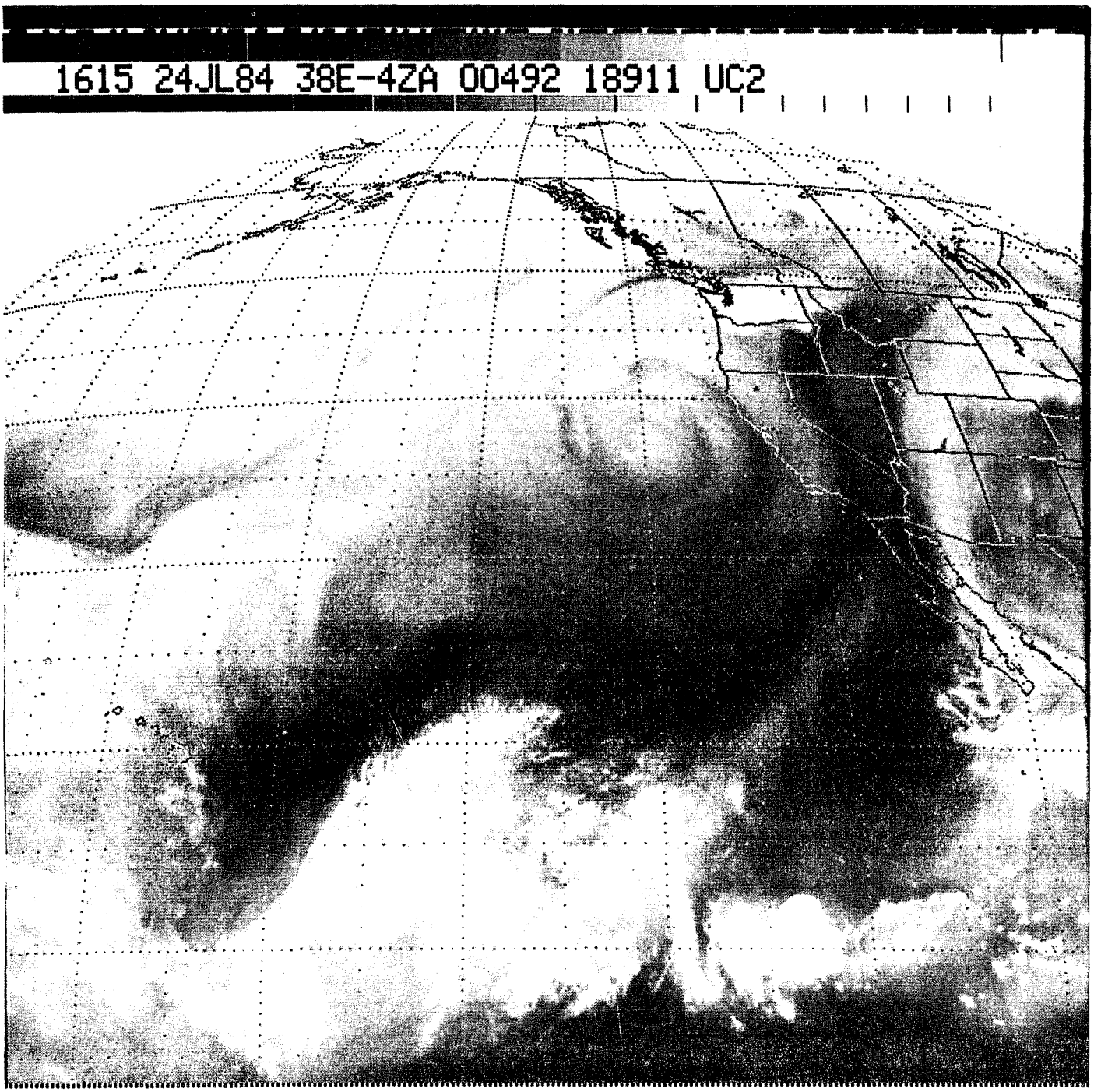

Figure 26
Water vapor satellite image
for 1615Z on July 24, 1984.

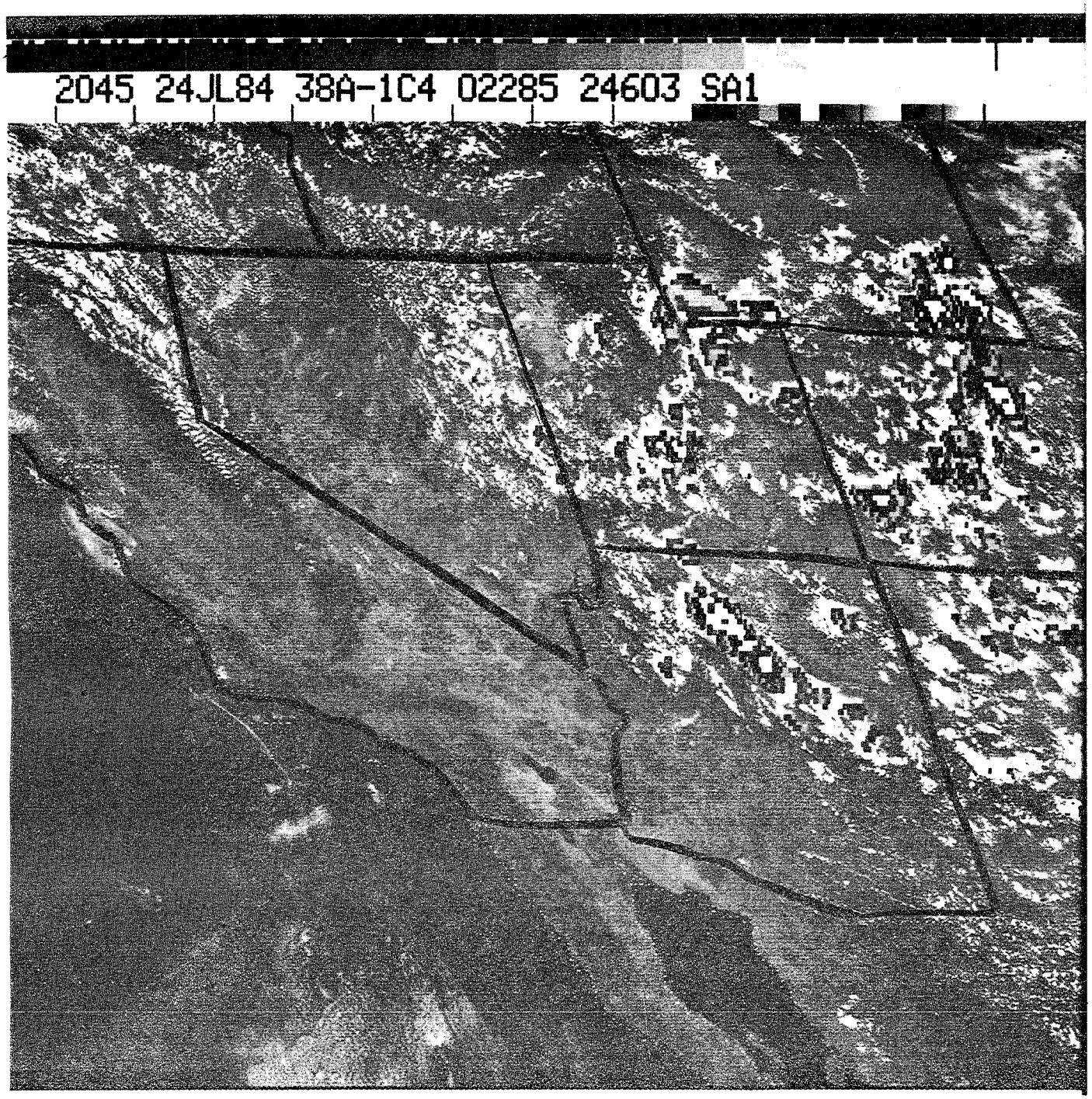

Figure 27
Enhanced visible satellite image for 2045Z on July 24, 1984.

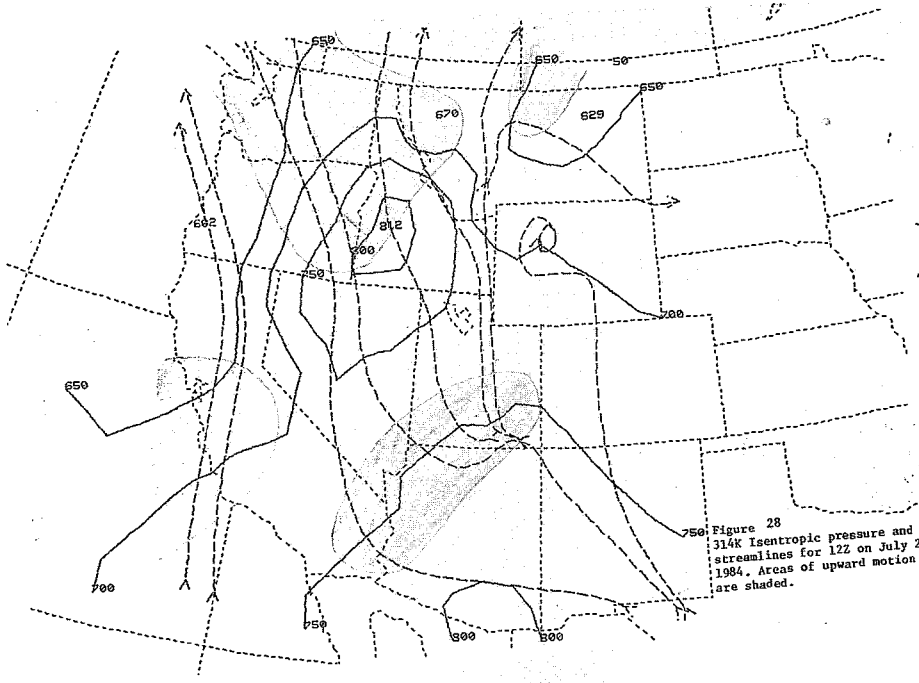

Figure 28
314K Isentropic pressure and streamlines for 12Z on July 25, 1984. Areas of upward motion are shaded.

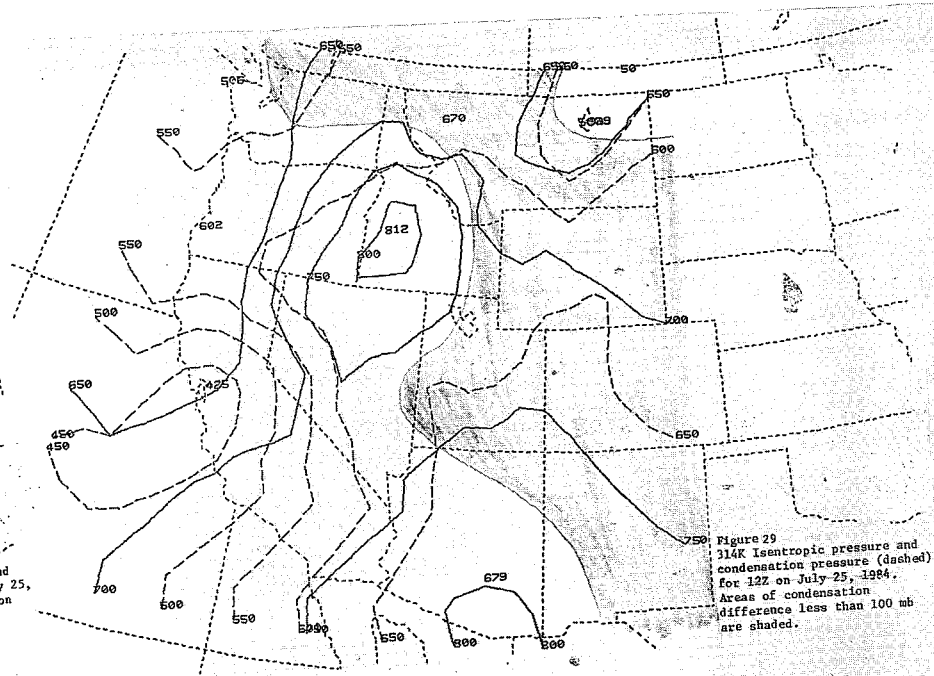

Figure 29
314K Isentropic pressure and condensation pressure (dashed) for 12Z on July 25, 1984. Areas of condensation difference less than 100 mb are shaded.

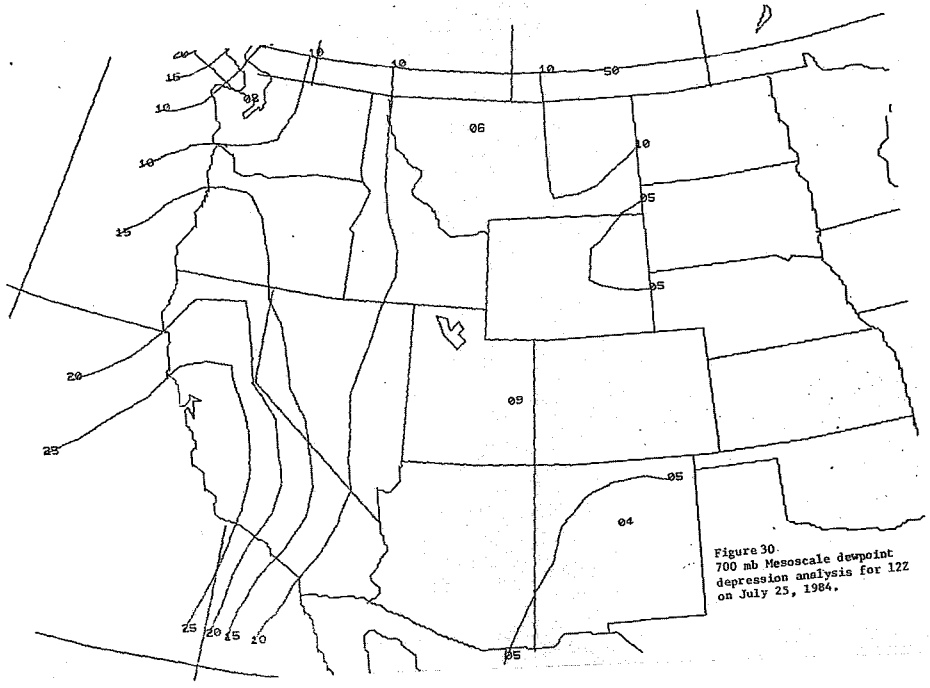

Figure 30
700 mb Mesoscale dewpoint depression analysis for 12Z on July 25, 1984.

Figure 31
700 mb Mesoscale temperature analysis for 12Z on July 25, 1984.

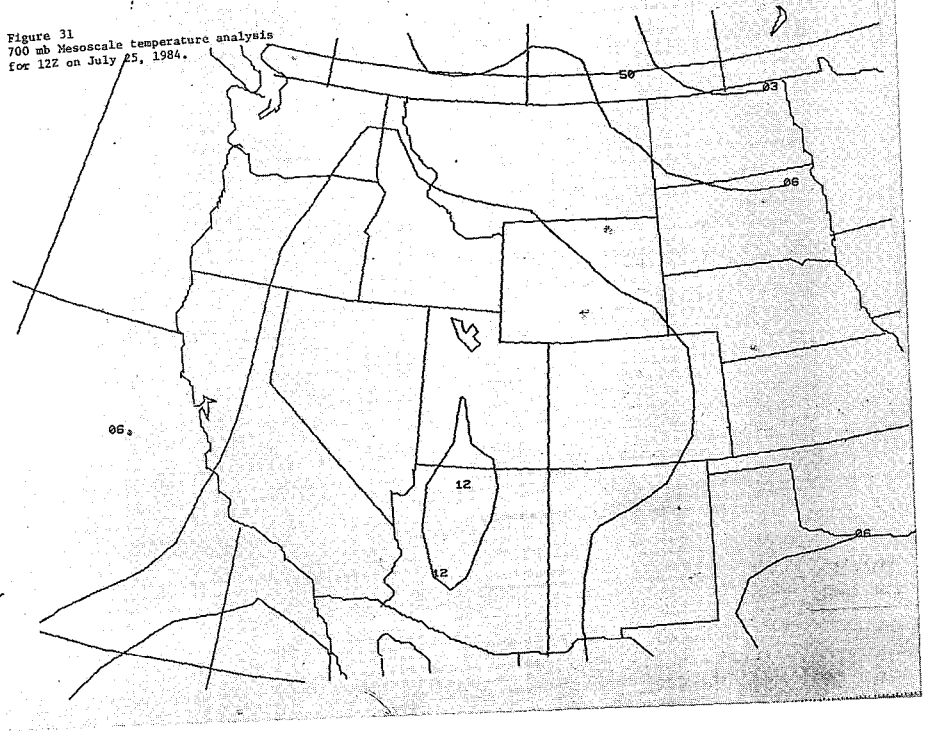

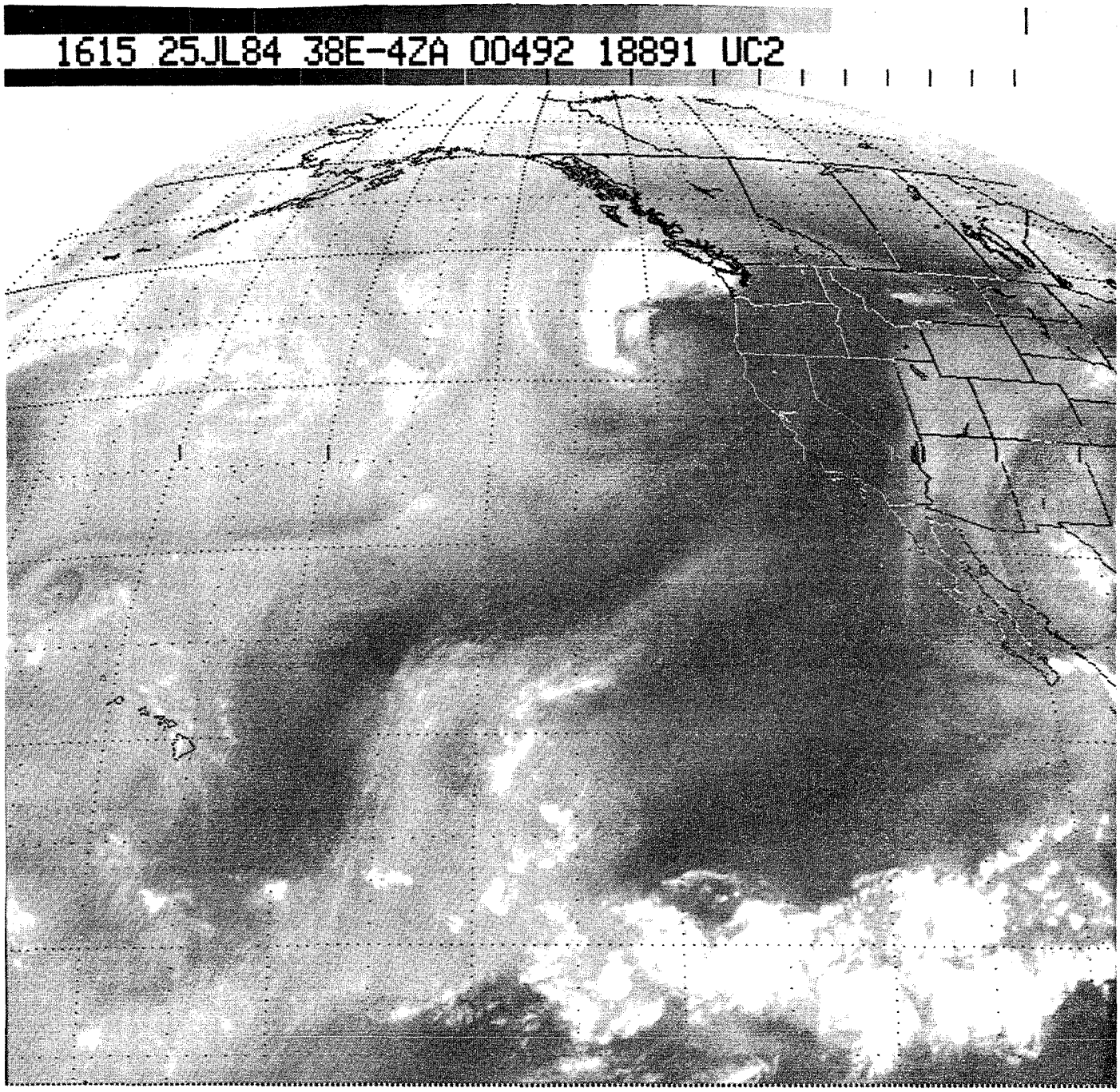

Figure 32
Water vapor satellite image for 1615Z on July 25, 1984.

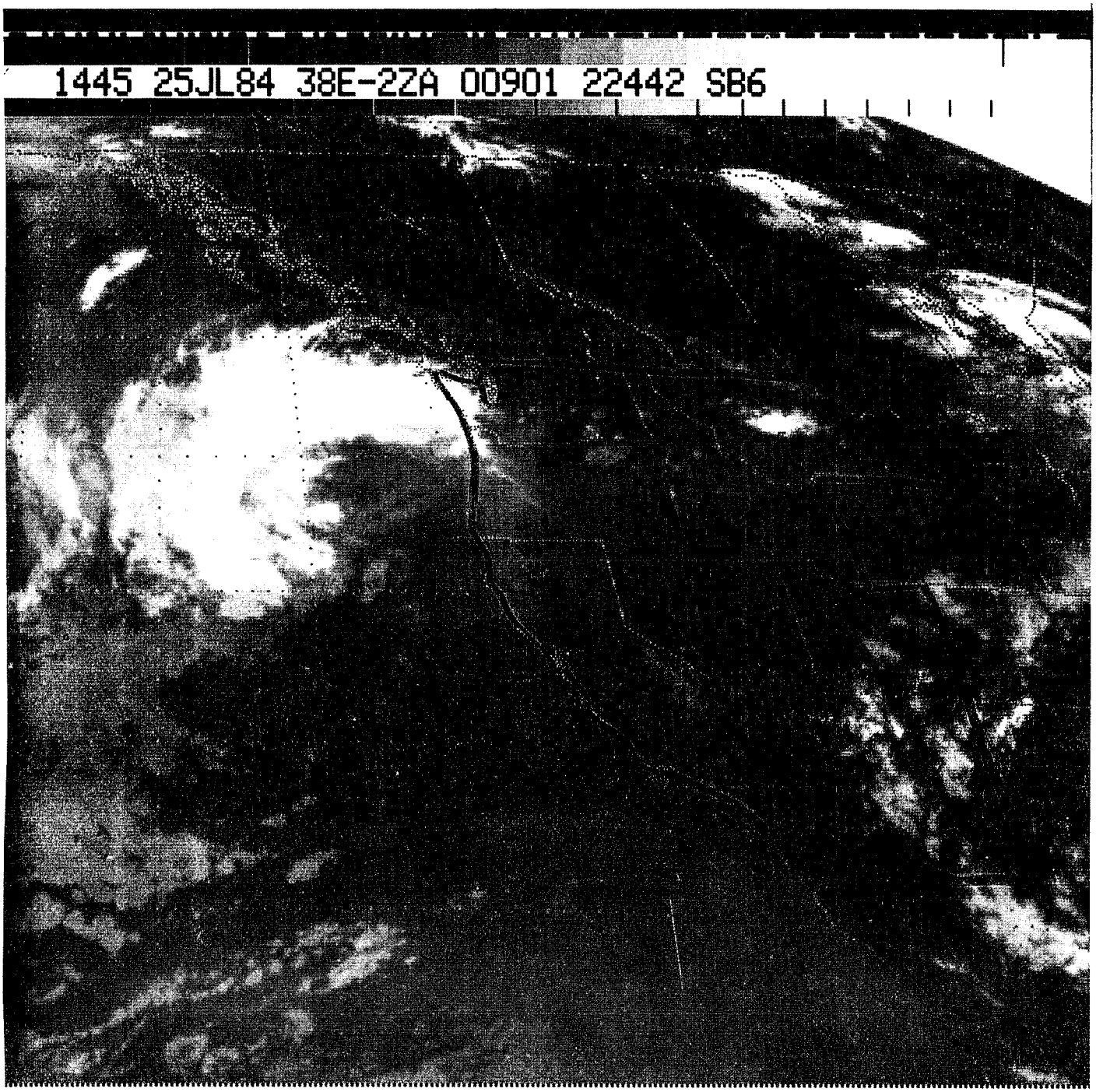

Figure 33
IR satellite image for
1445Z on July 25, 1984.

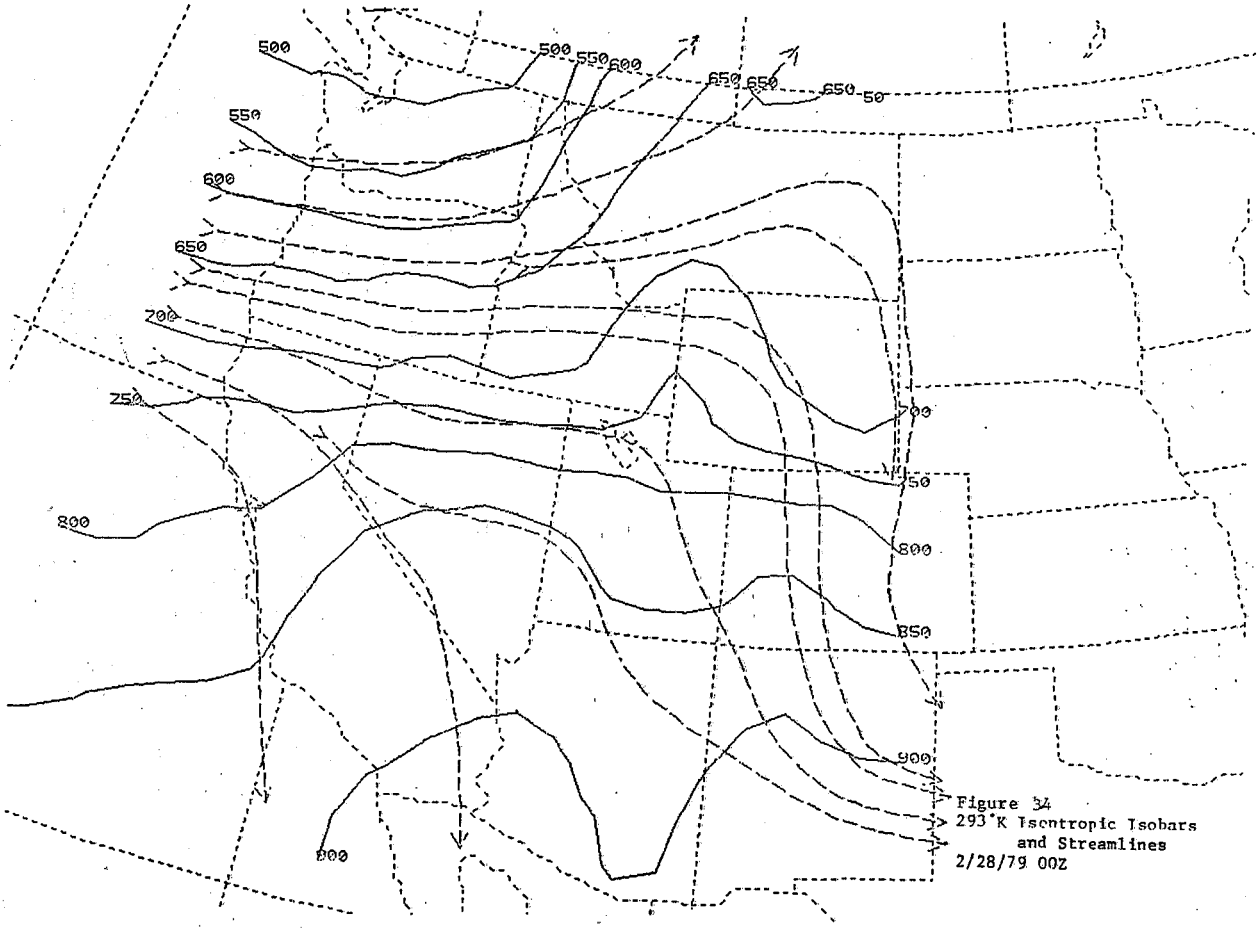

Figure 34
293°K Isentropic Isobars
and Streamlines
2/28/79 00Z

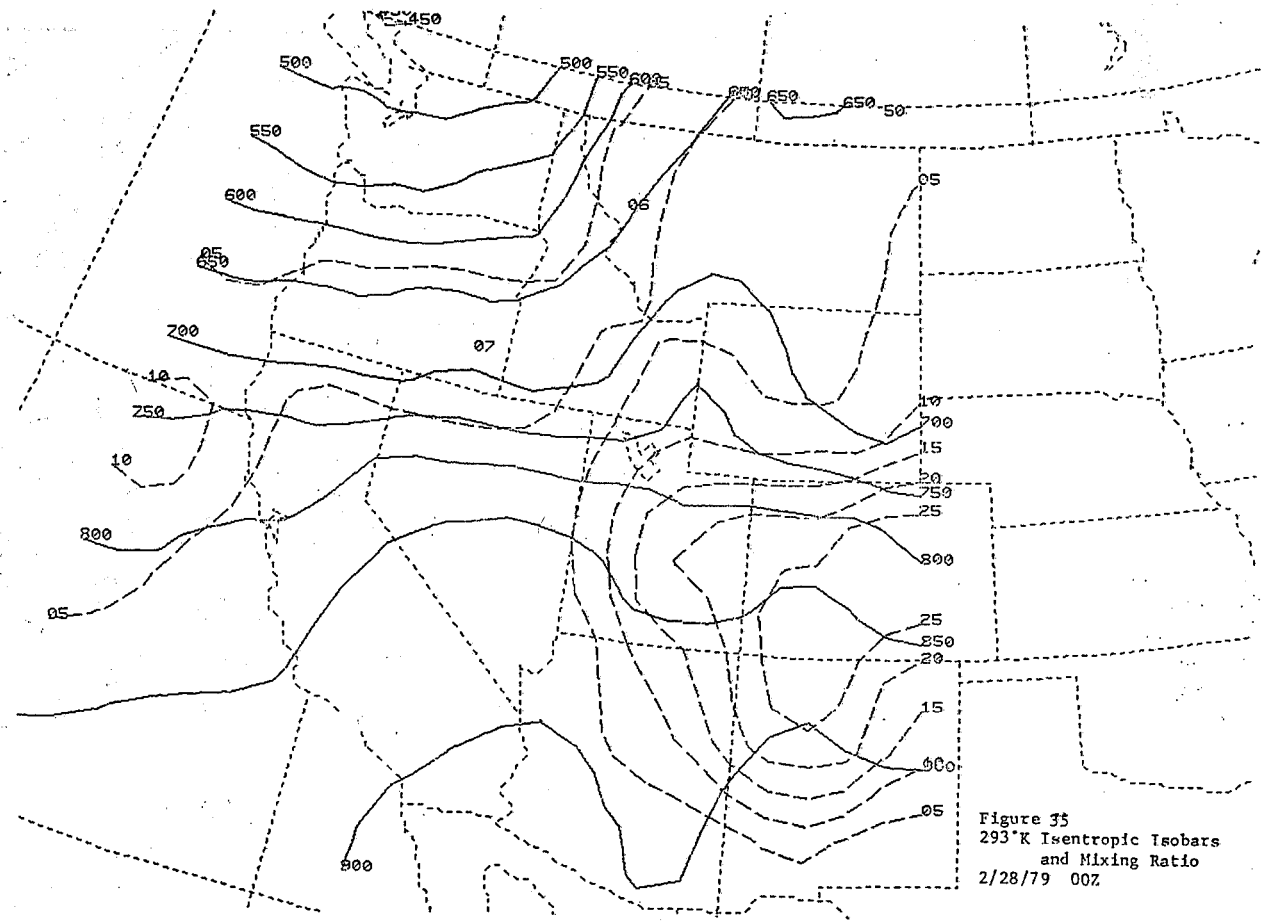

Figure 35
293°K Isentropic Isobars
and Mixing Ratio
2/28/79 00Z

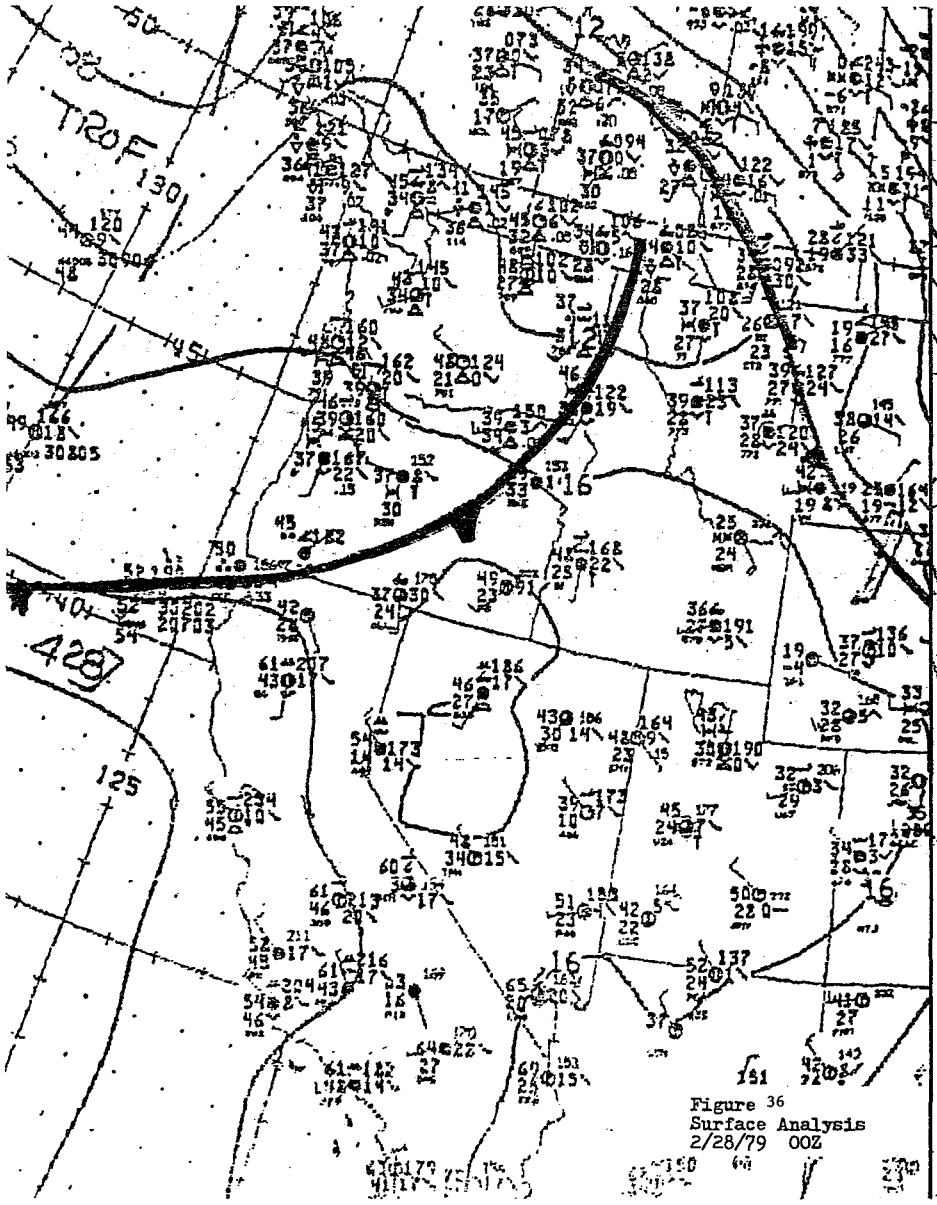

Figure 36
Surface Analysis
2/28/79 00Z

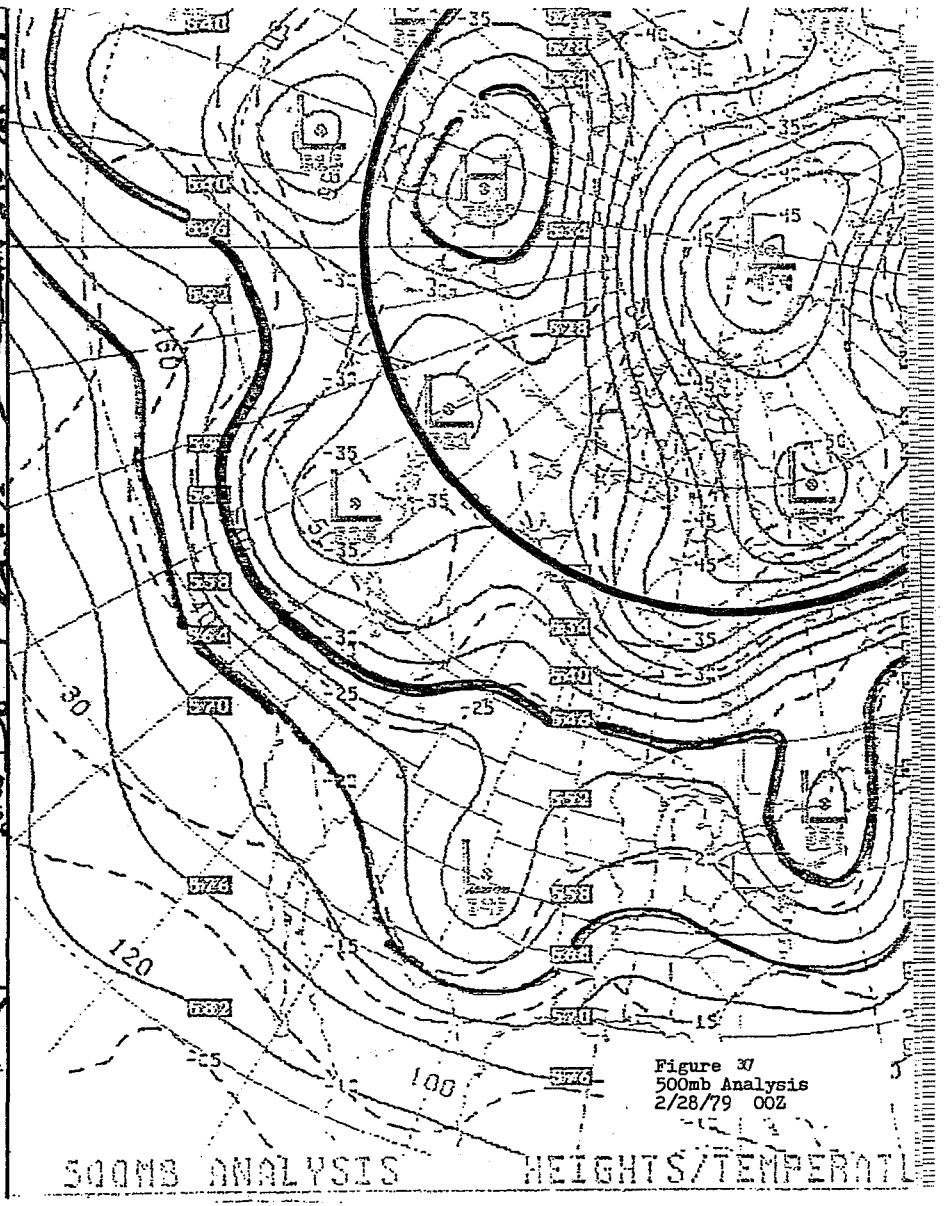

Figure 37
500mb Analysis
2/28/79 00Z

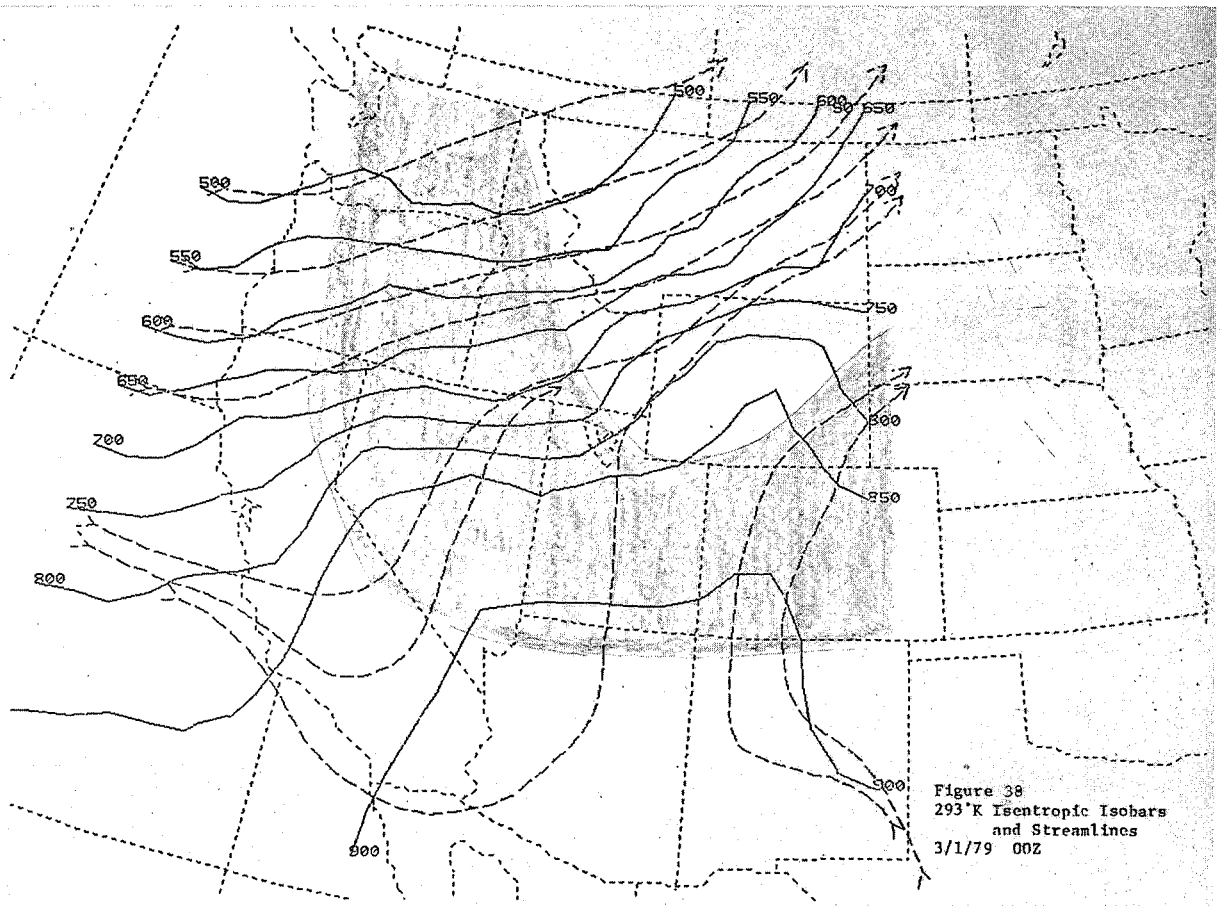

Figure 38
293°K Isentropic Isobars
and Streamlines
3/1/79 00Z

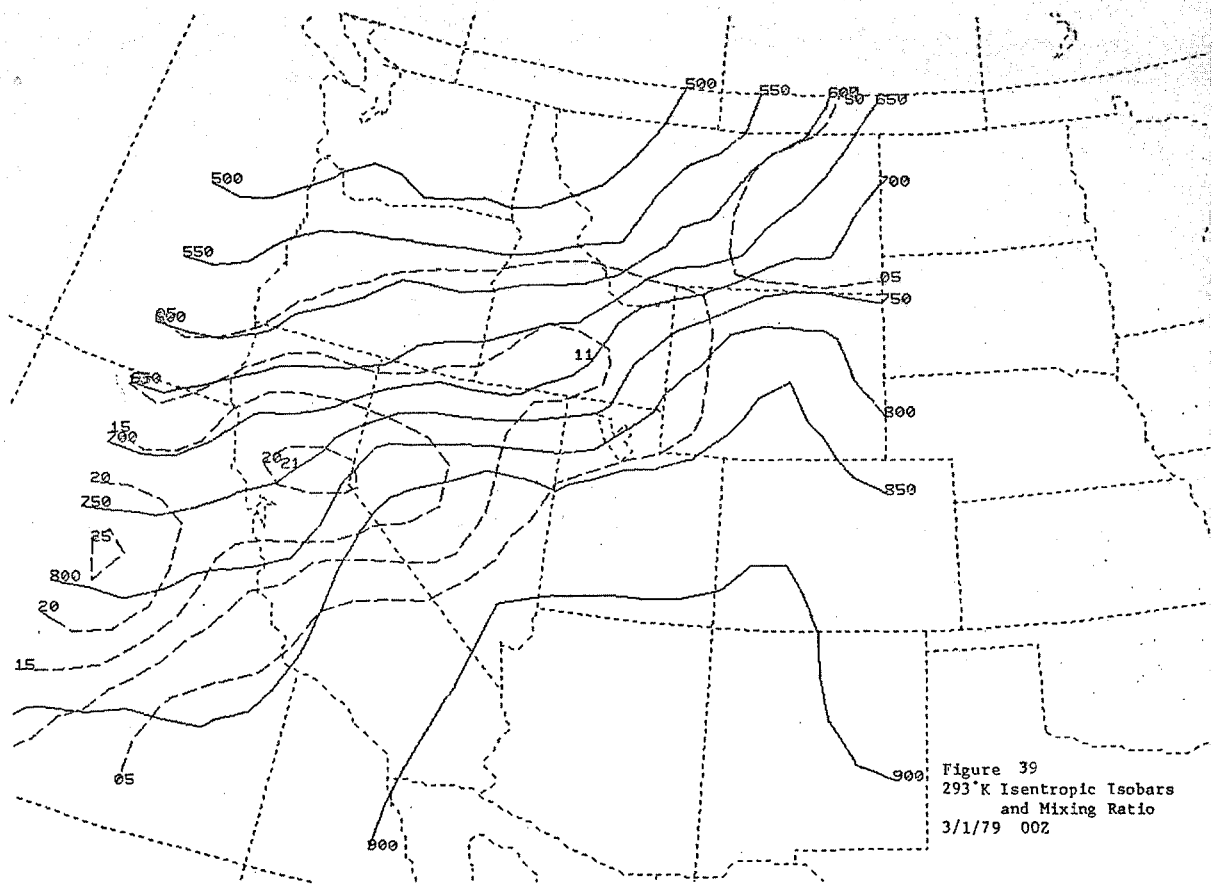

Figure 39
293°K Isentropic Isobars
and Mixing Ratio
3/1/79 00Z

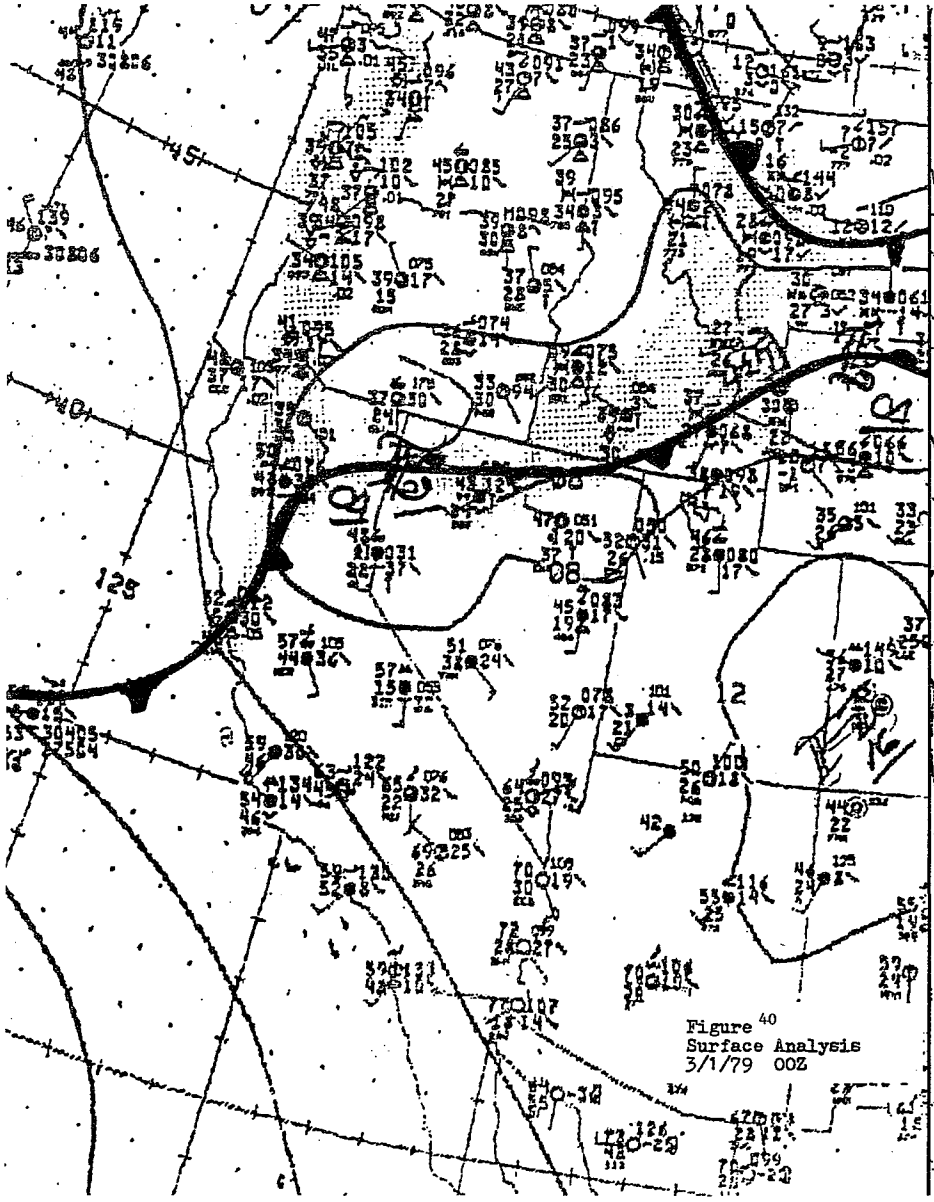

Figure 40
Surface Analysis
3/1/79 00Z

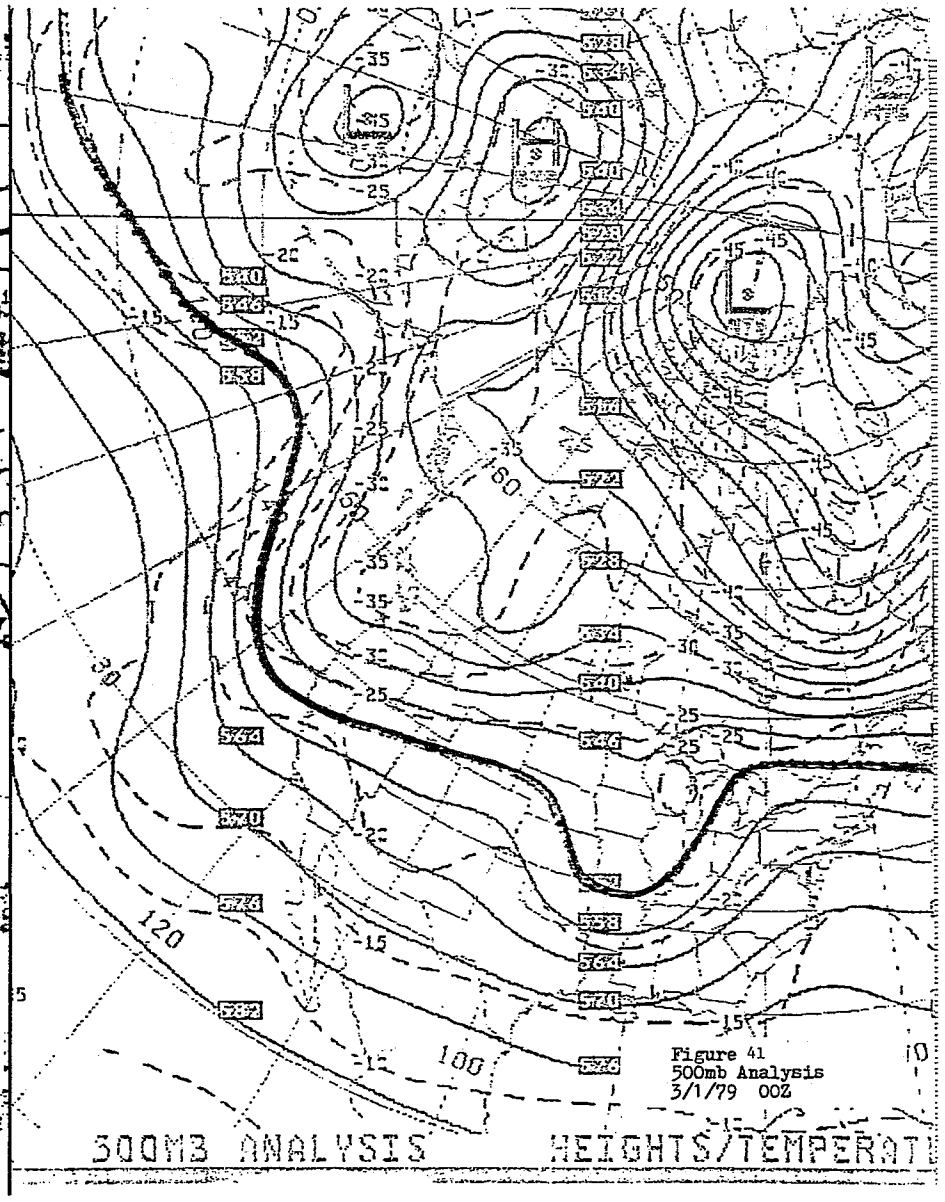

Figure 41
500mb Analysis
3/1/79 00Z

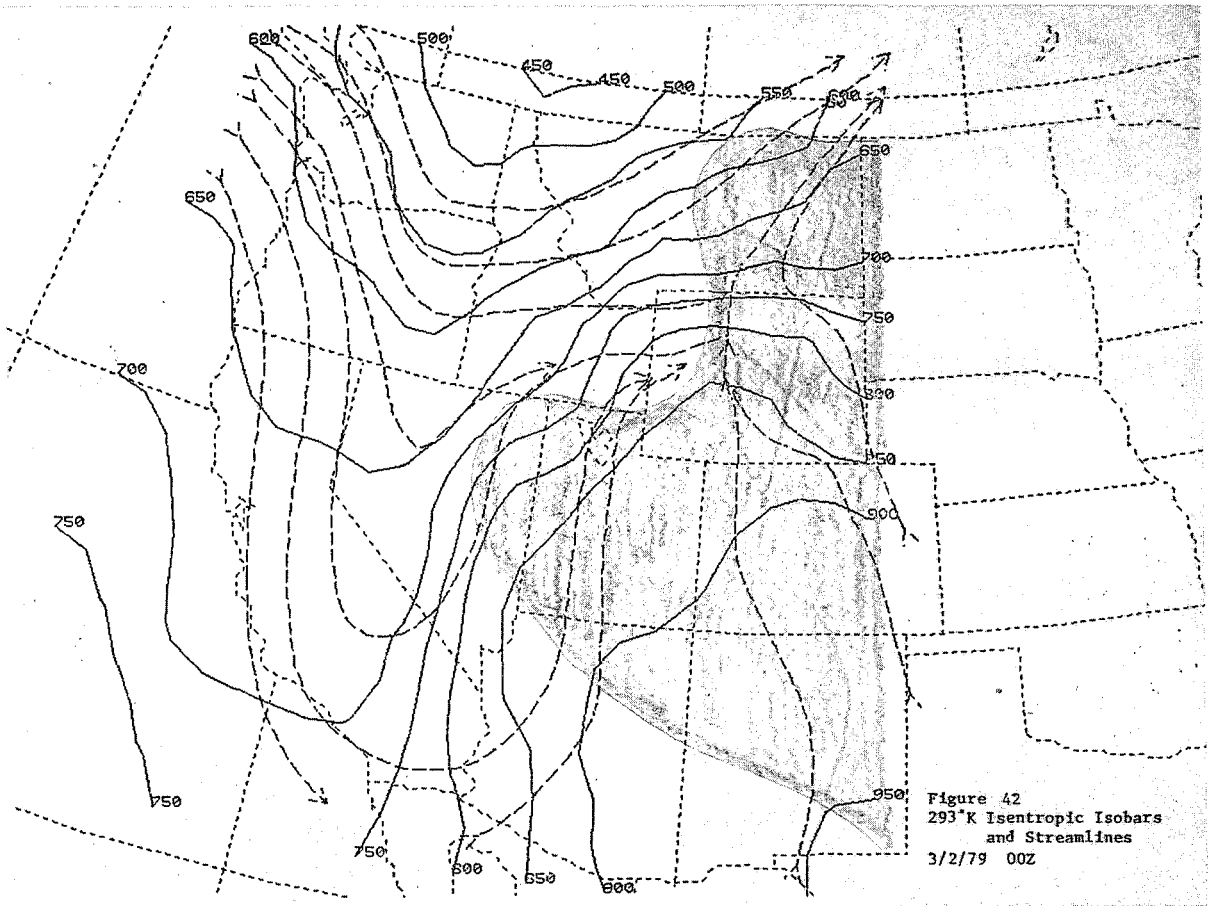

Figure 42
293°K Isentropic Isobars
and Streamlines
3/2/79 00Z

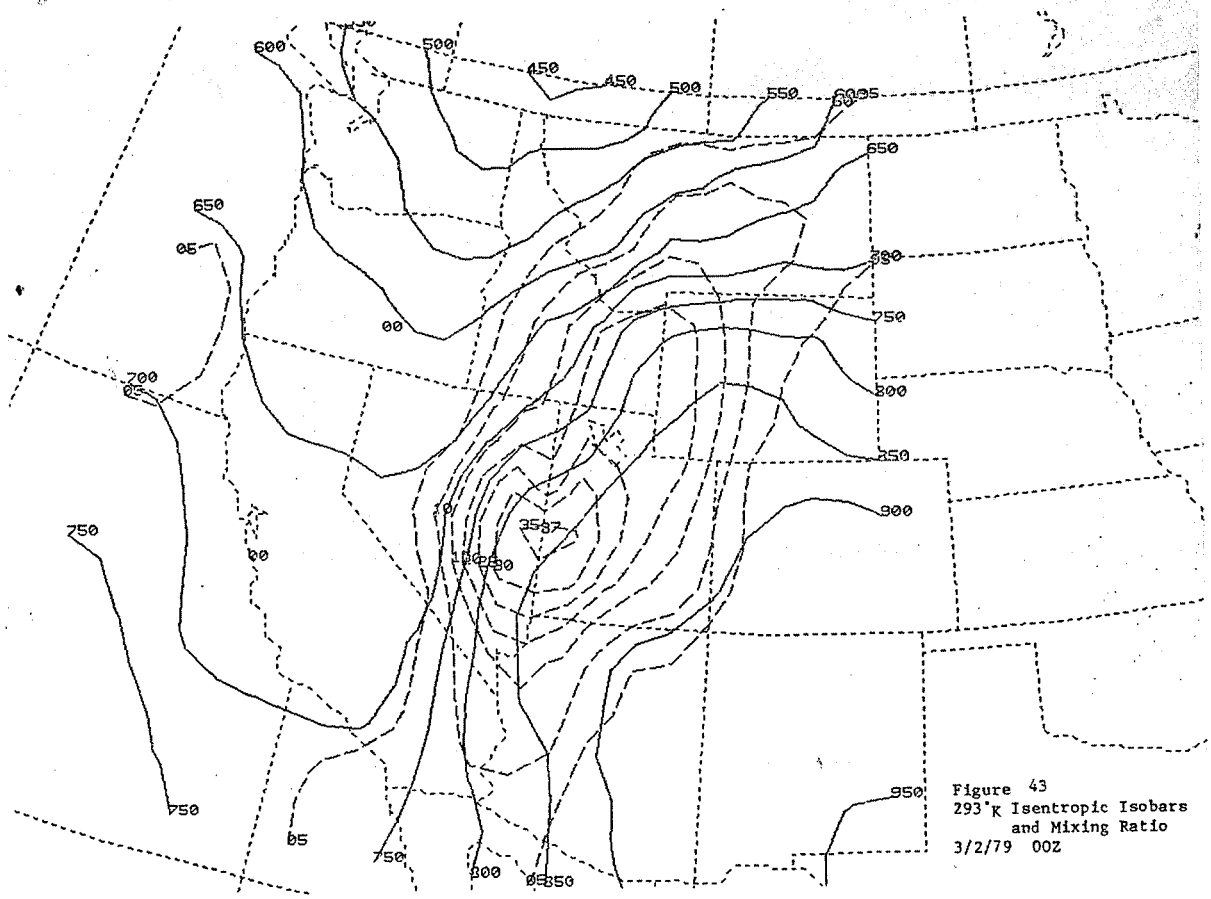

Figure 43
293°K Isentropic Isobars
and Mixing Ratio
3/2/79 00Z

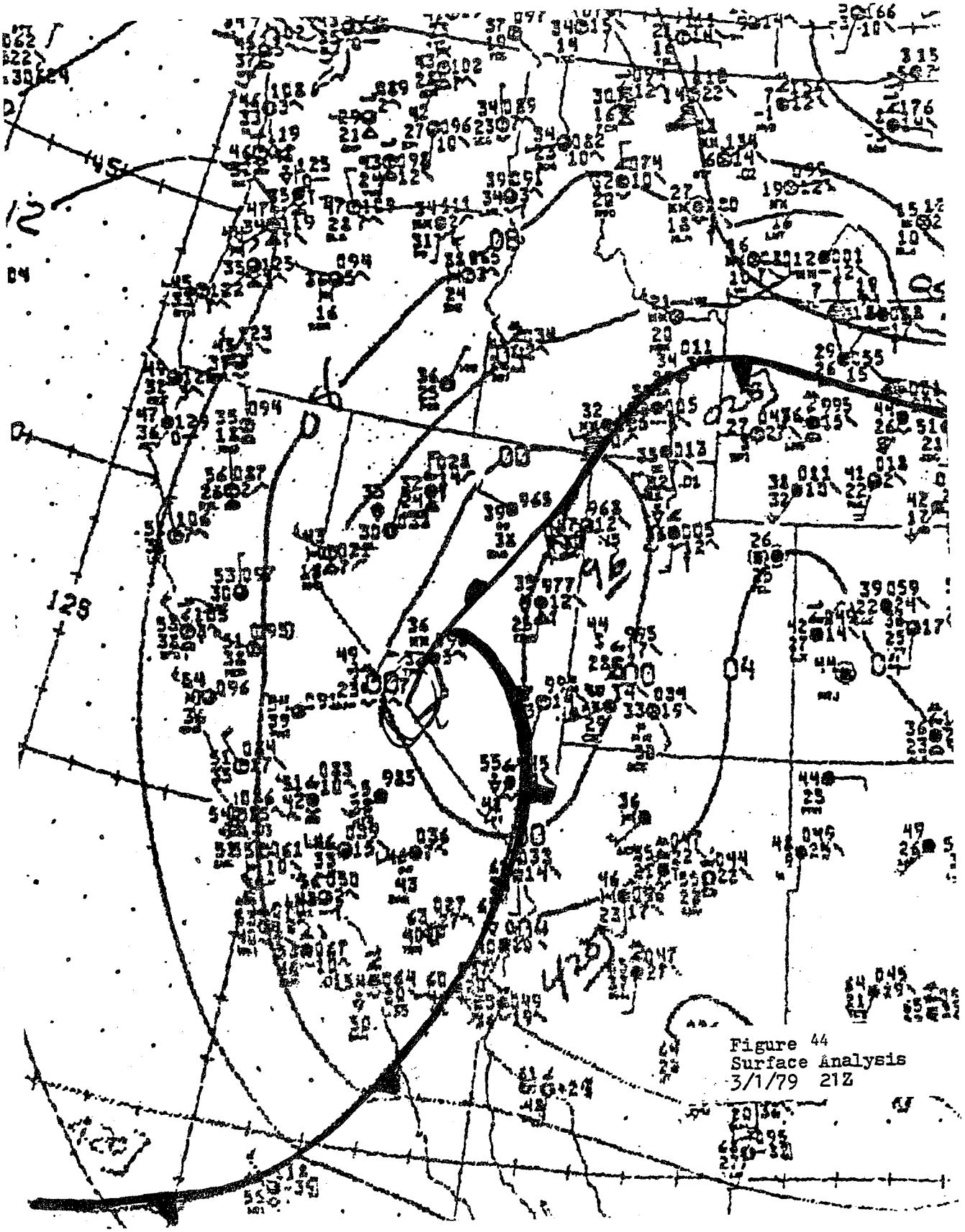

Figure 44
Surface Analysis
3/1/79 21Z

NOAA Technical Memoranda NWS WR: (Continued)

121 Climatological Prediction of Cumulonimbus Clouds in the Vicinity of the Yucca Flat Weather Station. R. F. Quiring, June 1977. (PB-271-704/AS)
122 A Method for Transforming Temperature Distribution to Normality. Morris S. Webb, Jr., June 1977. (PB-271-742/AS)
124 Statistical Guidance for Prediction of Eastern North Pacific Tropical Cyclone Motion - Part I. Charles J. Neumann and Preston W. Leftwich, August 1977. (PB-272-661)
125 Statistical Guidance on the Prediction of Eastern North Pacific Tropical Cyclone Motion - Part II. Preston W. Leftwich and Charles J. Neumann, August 1977. (PB-273-155/AS)
127 Development of a Probability Equation for Winter-Type Precipitation Patterns in Great Falls, Montana. Kenneth B. Mielke, February 1978.(PB-281-387/AS)
128 Hand Calculator Program to Compute Parcel Thermal Dynamics. Dan Gudgel, April 1978. (PB-283-080/AS)
129 Fire Whirls. David W. Goens, May 1978. (PB-283-866/AS)
130 Flash-Flood Procedure. Ralph C. Hatch and Gerald Williams, May 1978. (PB-286-014/AS)
131 Automated Fire-Weather Forecasts. Mark A. Mollner and David E. Olsen, September 1978. (PB-289-916/AS)
132 Estimates of the Effects of Terrain Blocking on the Los Angeles WSR-74C Weather Radar. R. G. Pappas, R. Y. Lee, B. W. Finke, October 1978.(PB289767/AS)
133 Spectral Techniques in Ocean Wave Forecasting. John A. Jannuzzi, October 1978. (PB291317/AS)
134 Solar Radiation. John A. Jannuzzi, November 1978. (PB291195/AS)
135 Application of a Spectrum Analyzer in Forecasting Ocean Swell in Southern California Coastal Waters. Lawrence P. Kierulff, January 1979. (PB292716/AS)
136 Basic Hydrologic Principles. Thomas L. Dietrich, January 1979. (PB292247/AS)
137 LFM 24-Hour Prediction of Eastern Pacific Cyclones Refined by Satellite Images. John R. Zimmerman and Charles P. Ruscha, Jr., Jan. 1979. (PB294324/AS)
138 A Simple Analysis/Diagnosis System for Real-Time Evaluation of Vertical Motion. Scott Heflick and James R. Fors, February 1979. (PB294216/AS)
139 Aids for Forecasting Minimum Temperature in the Wenatchee Frost District. Robert S. Robinson, April 1979. (PB298339/AS)
140 Influence of Cloudiness on Summertime Temperatures in the Eastern Washington Fire Weather District. James Holcomb, April 1979. (PB298674/AS)
141 Comparison of LFM and NFM Precipitation Guidance for Nevada During Doreen. Christopher Hill, April 1979. (PB298613/AS)
142 The Usefulness of Data from Mountaintop Fire Lookout Stations in Determining Atmospheric Stability. Jonathan W. Corey, April 1979. (PB298899/AS)
143 The Depth of the Marine Layer at San Diego as Related to Subsequent Cool Season Precipitation Episodes in Arizona. Ira S. Brenner, May 1979. (PB298817/AS)
144 Arizona Cool Season Climatological Surface Wind and Pressure Gradient Study. Ira S. Brenner, May 1979. (PB298900/AS)
145 On the Use of Solar Radiation and Temperature Models to Estimate the Snap Bean Maturity Date in the Willamette Valley. Earl M. Bates, August 1979. (PB80-160971)
146 The BART Experiment. Morris S. Webb, October 1979. (PB80-155112)
147 Occurrence and Distribution of Flash Floods in the Western Region. Thomas L. Dietrich, December 1979. (PB80-160344)
149 Misinterpretations of Precipitation Probability Forecasts. Allan H. Murphy, Sarah Lichtenstein, Baruch Fischhoff, and Robert L. Winkler, February 1980. (PB80-174576)
150 Annual Data and Verification Tabulation - Eastern and Central North Pacific Tropical Storms and Hurricanes 1979. Emil B. Gunther and Staff, EPHC, April 1980. (PB80-220486)
151 NMC Model Performance in the Northeast Pacific. James E. Overland, PMEL-ERL, April 1980. (PB80-196033)
152 Climate of Salt Lake City, Utah. Wilbur E. Figgins, October 1984, 2nd Revision.
153 An Automatic Lightning Detection System in Northern California. James E. Rea and Chris E. Fontana, June 1980. (PB80-225592)
154 Regression Equation for the Peak Wind Gust 6 to 12 Hours in Advance at Great Falls During Strong Downslope Wind Storms. Michael J. Oard, July 1980. (PB81-108367)
155 A Raininess Index for the Arizona Monsoon. John H. TenHarkel, July 1980. (PB81-106494)
156 The Effects of Terrain Distribution on Summer Thunderstorm Activity at Reno, Nevada. Christopher Dean Hill, July 1980. (PB81-102501)
157 An Operational Evaluation of the Scofield/Oliver Technique for Estimating Precipitation Rates from Satellite Imagery. Richard Ochoa, August 1980. (PB81-108227)
158 Hydrology Practicum. Thomas Dietrich, September 1980. (PB81-134033)
159 Tropical Cyclone Effects on California. Arnold Court, October 1980. (PB81-133779)
160 Eastern North Pacific Tropical Cyclone Occurrences During Intraseasonal Periods. Preston W. Leftwich and Gail M. Brown, February 1981. (PB81-205494)
161 Solar Radiation as a Sole Source of Energy for Photovoltaics in Las Vegas, Nevada, for July and December. Darryl Randerson, April 1981. (PB81-224503)
162 A Systems Approach to Real-Time Runoff Analysis with a Deterministic Rainfall-Runoff Model. Robert J. C. Burnash and R. Larry Ferral, April 1981. (PB81-224495)
163 A Comparison of Two Methods for Forecasting Thunderstorms at Luke Air Force Base, Arizona. Lt. Colonel Keith R. Cooley, April 1981. (PB81-225393)
164 An Objective Aid for Forecasting Afternoon Relative Humidity Along the Washington Cascade East Slopes. Robert S. Robinson, April 1981. (PB81-230378)
165 Annual Data and Verification Tabulation, Eastern North Pacific Tropical Storms and Hurricanes 1980. Emil B. Gunther and Staff, May 1981. (PB82-230336)
166 Preliminary Estimates of Wind Power Potential at the Nevada Test Site. Howard G. Booth, June 1981. (PB82-127036)
167 ARAP User's Guide. Mark Mathewson, July 1981. (revised September 1981). (PB82-196783)
168 Forecasting the Onset of Coastal Gales Off Washington-Oregon. John R. Zimmerman and William D. Burton, August 1981. (PB82-127051)
169 A Statistical-Dynamical Model for Prediction of Tropical Cyclone Motion in the Eastern North Pacific Ocean. Preston W. Leftwich, Jr., October 1981.
170 An Enhanced Plotter for Surface Airways Observations. Andrew J. Spry and Jeffrey L. Anderson, October 1981. (PB82-153883)
171 Verification of 72-Hour 500-mb Map-Type Predictions. R. F. Quiring, November 1981. (PB82-158098)
172 Forecasting Heavy Snow at Wenatchee, Washington. James W. Holcomb, December 1981. (PB82-177783)
173 Central San Joaquin Valley Type Maps. Thomas R. Crossan, December 1981. (PB82-196064)
174 ARAP Test Results. Mark A. Mathewson, December 1981. (PB82-193103)
175 Annual Data and Verification Tabulation Eastern North Pacific Tropical Storms and Hurricanes 1981. Emil B. Gunther and Staff, June 1982.(PB82-252420)
176 Approximations to the Peak Surface Wind Gusts from Desert Thunderstorms. Darryl Randerson, June 1982. (PB82-253089)
177 Climate of Phoenix, Arizona. Robert J. Schmidli, April 1969 (revised March 1983). (PB83246801)
178 Annual Data and Verification Tabulation, Eastern North Pacific Tropical Storms and Hurricanes 1982. E. B. Gunther, June 1983. (PB85 106078)
179 Stratified Maximum Temperature Relationships Between Sixteen Zone Stations in Arizona and Respective Key Stations. Ira S. Brenner, June 1983. (PB83-249904)
180 Standard Hydrologic Exchange Format (SHEF) Version I. Phillip A. Pasteries, Vernon C. Bissel, David G. Bennett, August, 1983.(PB85 106052)
181 Quantitative and Spacial Distribution of Winter Precipitation Along Utah's Wasatch Front. Lawrence B. Dunn, August, 1983. (PB85 106912)
182 500 Millibar Sign Frequency Teleconnection Charts - Winter. Lawrence B. Dunn, December, 1983.
183 500 Millibar Sign Frequency Teleconnection Charts - Spring. Lawrence B. Dunn, January, 1984.
184 Collection and Use of Lightning Strike Data in the Western U.S. During Summer 1983. Glenn Rasch and Mark Mathewson, February, 1984.
185 500 Millibar Sign Frequency Teleconnection Charts - Summer. Lawrence B. Dunn, March 1984.
186 Annual Data and Verification Tabulation Eastern North Pacific Tropical Storms and Hurricanes 1983. E. B. Gunther, March 1984.
187 500 Milibar Sign Frequency Teleconnection Charts - Fall. Lawrence B. Dunn, May 1984.

NOAA SCIENTIFIC AND TECHNICAL PUBLICATIONS

The National Oceanic and Atmospheric Administration was established as part of the Department of Commerce on October 3, 1970. The mission responsibilities of NOAA are to assess the socioeconomic impact of natural and technological changes in the environment and to monitor and predict the state of the solid Earth, the oceans and their living resources, the atmosphere, and the space environment of the Earth.

The major components of NOAA regularly produce various types of scientific and technical information in the following kinds of publications:

PROFESSIONAL PAPERS — Important definitive research results, major techniques, and special investigations.

CONTRACT AND GRANT REPORTS — Reports prepared by contractors or grantees under NOAA sponsorship.

ATLAS — Presentation of analyzed data generally in the form of maps showing distribution of rainfall, chemical and physical conditions of oceans and atmosphere, distribution of fishes and marine mammals, ionospheric conditions, etc.

TECHNICAL SERVICE PUBLICATIONS — Reports containing data, observations, instructions, etc. A partial listing includes data serials; prediction and outlook periodicals; technical manuals, training papers, planning reports, and information serials; and miscellaneous technical publications.

TECHNICAL REPORTS — Journal quality with extensive details, mathematical developments, or data listings.

TECHNICAL MEMORANDUMS — Reports of preliminary, partial, or negative research or technology results, interim instructions, and the like.

Information on availability of NOAA publications can be obtained from:

ENVIRONMENTAL SCIENCE INFORMATION CENTER (D822)
ENVIRONMENTAL DATA AND INFORMATION SERVICE
NATIONAL OCEANIC AND ATMOSPHERIC ADMINISTRATION
U.S. DEPARTMENT OF COMMERCE

6009 Executive Boulevard
Rockville, MD 20852